



**SINGLE AND DOUBLE LAYER BULK HETEROJUNCTION ORGANIC
SOLAR CELL**

MSc Dissertation

by

MPUMELELO HOWARD HLONGWANE

Submitted in partial fulfilment of the academic requirements of

Master of Science

in

Physics

School of Chemistry and Physics

College of Agriculture, Engineering and Science

University of KwaZulu-Natal

Pietermaritzburg, Campus

South Africa

November 2015

Contents

1	Introduction	1
2	Organic semiconductors	4
2.1	The general properties of organic semiconductor	6
3	Charge transport properties	8
3.1	Charge transport theory	8
3.2	Current Density Equation	8
3.3	Space charge-limited current	9
3.4	Thermionic emission and Field emission Theory	10
3.4.1	Thermionic emission theory	10
3.4.2	Field emission theory: Background	11
3.5	Injection limited current	14
4	Characterization of a Solar Cell device	15
4.1	Open-circuit voltage (V_{oc})	16
5	Organic Solar Cell (OSC)	19
5.1	Mechanism of charge generation in OSC	20
5.1.1	Light absorption	20
5.1.2	Exciton diffusion	20
5.1.3	Charge separation	21
5.1.4	Charge transport in organic solar cell	22
5.1.5	Charge collection	24
5.2	Organic Solar Cell (OSC) Device Architecture	24
5.2.1	Single layer device	24

5.2.2	Bilayer device	26
5.2.3	Bulk heterojunction (BHJ) device	27
6	Experimental	30
6.1	Sample Preparation	30
7	Results and Discussion	33
7.1	Optical Absorption Properties	33
7.2	Electrical properties	35
7.3	Charge transport properties	39
7.4	Morphology of P3HT:PCBM	43
8	Conclusion	44

List of Figures

2.1	(a)Simplest π -conjugated electron system (where σ and π bonds are shown for ethylene), (b) depicts π -conjugated molecules energy level.	4
2.2	Organic semiconductors molecular structure [1].	5
2.3	Organic solar cell (OSC) depicting the bulk heterojunction device [1].	7
3.1	Schematic diagram representing two terminals of the voltage source across a device of thickness L [2].	9
3.2	Dark current showing various transport phenomena [3].	14
4.1	Typical J-V curve for bulk heterojunction organic solar cell device under both dark and illumination conditions [4].	17
5.1	Charge transport by hopping between localised states with a gaussian energy distribution and disordered system of polymer medium [5].	23
5.2	Configurations of single layer device [6].	25
5.3	Configurations of bilayer device with planar heterojunction [4].	26
5.4	Configurations of bulk heterojunction organic solar cell device [7].	28
6.1	PI-KEM LTD Spin-Coater KW-4A used to spin-coat photo-active layers on the samples.	31
6.2	Chemical structures for molecules used in the preparations of the photo-active layers [8].	31
6.3	Edward Auto 306 vacuum deposition chamber unit used to deposit LiF and Al on the samples.	32
7.1	UV-Vis absorption spectra for all our experimental samples.	34

7.2	The J-V characteristics of BHJ OSC with photo-active layers of PTB7:PCBM and P3HT:PCBM/PTB7:PCBM blends. d1 to d5 represents the number of diodes on the device for both single and double layer.	36
7.3	J-V curve under dark condition for both single and double layer.	37
7.4	Schematic representation of $\ln(J)$ -V curve under dark condition, (a) is for binary molecular blend, (b) is for double layer molecular blend, where the behaviour on charge transport is the same for both (a) and (b).	39
7.5	$\ln(J)$ vs Voltage fitted with space charge-limited current equation.	41
7.6	SEM image for photo-active layer of BHJ solar cell fabricated under laboratory ambient conditions.	43

List of Tables

7.1	Best performing sample that was produced in the laboratory under illumination for (PTB7:PCBM) and the $P_{in} = 0.100 \text{ Wcm}^{-2}$ and the $Area = 0.0657 \text{ cm}^2$	37
7.2	Best performing sample that was produced in the laboratory under illumination for (P3HT:PCBM/PTB7:PCBM) and the $P_{in} = 0.100 \text{ Wcm}^{-2}$ and the $Area = 0.0957 \text{ cm}^2$	38
7.3	Best fitted results for dark current single layer (PTB7:PCBM) in SCLC region 3.	42
7.4	Best fitted results for dark current double layer (P3HT:PCBM/PTB7:PCBM) in SCLC region 3.	42
8.1	Best performing sample that was produced in the laboratory under illumination for (PTB7:PCBM) after 30 minutes and the $P_{in} = 0.100 \text{ Wcm}^{-2}$ and the $Area = 0.0657 \text{ cm}^2$	46
8.2	Best performing sample that was produced in the laboratory under illumination for (PTB7:PCBM/P3HT:PCBM) and the $P_{in} = 0.100 \text{ Wcm}^{-2}$ and the $Area = 0.1157 \text{ cm}^2$	46
8.3	Best performing sample that was produced in the laboratory under illumination for (P3HT:PCBM/PTB7:PCBM) after 30 minutes and the $P_{in} = 0.100 \text{ Wcm}^{-2}$ and the $Area = 0.0957 \text{ cm}^2$	47
8.4	Best performing sample that was produced in the laboratory under illumination for (P3HT:PCBM/PTB7:PCBM) and the $P_{in} = 0.100 \text{ Wcm}^{-2}$ and the $Area = 0.0957 \text{ cm}^2$	47
8.5	Best performing sample that was produced in the laboratory under illumination for (P3HT:PCBM) and the $P_{in} = 0.100 \text{ Wcm}^{-2}$ and the $Area = 0.0657 \text{ cm}^2$	48

8.6	Best performing sample that was produced in the laboratory under illumination for (P3HT:PCBM after 30 minutes) and the $P_{in} = 0.100 \text{ Wcm}^{-2}$ and the $Area = 0.0657 \text{ cm}^2$	48
8.7	Best fitted results for dark current double layer blend (PTB7:PCBM/P3HT:PCBM) in SCLC region 3.	49
8.8	Best fitted results for dark current single layer blend (P3HT:PCBM) in SCLC region 3.	49

PREFACE

The research contained in this dissertation was completed by the candidate while based in the School of Chemistry and Physics of the College of Agriculture, Engineering and Science, University of KwaZulu-Natal, Pietermaritzburg Campus, South Africa. The research was financially supported by NRF.

The contents of this work have not been submitted in any form to another university and, except where the work of others is acknowledged in the text, the results reported are due to investigations by the candidate.

Signed: _____

Date: _____

DECLARATION : PLAGIARISM

I, MPUMELELO HOWARD HLONGWANE declare that:

- (i) the research reported in this dissertation, except where otherwise indicated or acknowledged, is my original work;
- (ii) this dissertation has not been submitted in full or in part for any degree or examination to any other university;
- (iii) this dissertation does not contain other persons data, pictures, graphs or other information, unless specifically acknowledged as being sourced from other persons;
- (iv) this dissertation does not contain other persons writing, unless specifically acknowledged as being sourced from other researchers. Where other written sources have been quoted, then:
 - a) their words have been re-written but the general information attributed to them has been referenced;
 - b) where their exact words have been used, their writing has been placed inside quotation marks, and referenced;
- (v) where I have used material for which publications followed, I have indicated in detail my role in the work;
- (vi) this dissertation is primarily a collection of material, prepared by myself, published as journal articles or presented as a poster and oral presentations at conferences. In some cases, additional material has been included;
- (vii) this dissertation does not contain text, graphics or tables copied and pasted from the Internet, unless specifically acknowledged, and the source being detailed in the dissertation and in the References sections.

Signed: _____

Date: _____

Abstract

Bulk heterojunction photovoltaic device based on the binary organic comprised of P3HT:PCBM and PTB7:PCBM with weight ratio of 1:1 and 1:1.5 respectively. We used these blends as a photo-active layer with different structures such as single layer of the P3HT:PCBM and PTB7:PCBM, as well as top-down and bottom-up as double layers of the two active layers respectively. These layers were deposited using two different simple and inexpensive techniques such as spin-coating and roll-to-roll (R2R) under ambient laboratory conditions. The current density-voltage (J-V) characteristics, optical and morphological properties were investigated. The J-V characteristics exhibited average of power conversion efficiency of 2.7% for single binary layer blend and 1.3% of double layer blend. The optical absorption band of a double layer binary blends was extended better than single layer. However, the device performance of the double layer was found too low due to poor charge transport processes in the medium. This is an encouraging development toward achieving low cost organic photovoltaic devices based on single layer ternary blend active layer.

ACKNOWLEDGMENTS

It had been the great two and a half years, filled with many challenges, so I would like to express my deepest appreciation to the following:

Firstly, I would like to thank the Almighty Lord for everything, without his grace I would not have made it this far.

Secondly, I would also like to thank my supervisor Prof. Genene Tessema Mola for his guidance, patience and encouragements when things got tough, so without him this research would not have been successful.

Thirdly, Ngithanda ukudlulisa ukubonga to all my family "oSangweni, Ngwane, Masumpa, Zikhali, oNduku zinobulongwe" especially my mom and dad for their tireless support, also would like to thank umama wo boys bami (uPhelelani and Phiwokuhle) for her support.

Fourthly, I would like to thank Mr. Karl Penzhorn and Mr. Ravin Sivraman the Physics technical staff noMaKhumalo, also would like thank Mr. Elhadi Arbab (PhD Candidate), and all my friends for being there for me.

Fifthly, I would like to thank the National Research Foundation (NRF) for their financial support toward my Masters degree.

Finally, I would like to express my deepest appreciation to the School of Chemistry and Physics for their support, also would like to thank the University of KwaZulu-Natal for giving me the opportunity to start my career.

Chapter 1

Introduction

Solar energy is known as sustainable energy source because of inexhaustible nature of solar radiation, and, solar energy conversion devices produce free of greenhouse effect electricity [9]. There are two major challenges facing the world today which are sustainable energy sources and environment pollution. It is impossible to separate these two issues because they are very connected to each other. The world is more and more dependant on the use of electricity because of the developing new technologies by which human society consumes a huge amount of energy (about 18.921 *TWh*) [10] for cooking, heating water, electric machines, gadgets and also their manufacturing facilities. Today, almost over 80% of the energy sources are obtained from burning of fossil fuels (i.e. oil, natural gases and coals), with the exception of 13% amount of electricity produced by water, nuclear, geothermic and wind power [10]. However, burning fossil fuels releases carbon dioxide and other gases causing many potential environmental problems (i.e. greenhouse effect). The largest greenhouse gas emitters in the world are fossil fuels. The most common means of producing electricity is when fossil fuels are being burnt at extremely high temperatures (combustion), but that gives problems because it results to heavy concentrations of pollution (air and water pollutants). Another major concern is that tons of greenhouse gases have been absorbed naturally by the atmosphere, but now it traps an extra 25% more of the sun's radiation and that may increase chances of global warming. Another issue is that, the size of fossil fuels deposit is decreasing quickly by consumption [10]. However, the energy required and environmental impact can be reduced on PV manufacturing [9]. There are two major concerns so far on environmental issues based on photovoltaics manufacturing, first one is to handle safely the gases which are used for sur-

face treatment or the growth of thin films (e.g. PH_3 and B_2H_6). Second one is the toxic components of semiconductor processing (e.g. Cd), although, a good progress in dealing with hazardous materials has been made by the electronics industry [9]. None-the-less, further investigation could lead to the replacement of toxic components and that would result on eliminating the concerns about the environmental risks of photovoltaics [9]. The best possible solution to consider is recycling in order to get the public to adopt the PV technologies [9]. Due to the increasing awareness surrounding global warming, the renewable energy seems to be the only alternative that produce the clean and harmful gas-free electricity. As a result, the big concern arises on how long will these non-renewable energy sources be readily available (hundreds or thousands years?). Therefore, there is a need to develop new technologies exploiting the alternative renewable and clean energy sources to supply the whole world with electricity without polluting the environment. Renewable energy sources have become a major research area which challenges the scientists in the twenty-first century [10].

Solar energy is the biggest renewable and clean energy source on earth that can be accessible almost everywhere and it is inexhaustible. The sun is rising over the horizon, circumnavigates the world and leaves behind 1.08×10^{18} kWh amount of energy everyday, which is much more than what the world needs to satisfy its electricity consumption for industry and households. However, it was impossible to convert even 0.001% of this daily solar radiation into electricity, and that would cover the energy consumptions for the whole year. Technology for converting solar radiation into electricity has been existing for decades, but it has been fabricated using inorganic semiconductors (silicon) [11]. Visible and infrared regions constitutes the majority of the emission of radiation among the total radiation emission. Therefore, most solar cells are designed to operate by harvesting electromagnetic radiations from visible and infrared regions of the solar spectrum. The conversion of electromagnetic radiation energy into electricity was first discovered by the French physicist Edmund Becquerel (1839) [11]. Becquerel observed that semiconductors when exposed to sunlight can generate direct current electricity and low voltage. Since then the idea of generating free charge carries by the means of electromagnetic radiation has been used for different purposes (i.e. solar cells). Solar cells made from inorganic semiconductors has been successful in the energy market. Silicon based processing for

solar cells fabrications is very expensive and not affordable to many people. But, organic semiconductors came into picture recently such as organic solar cells (OSCs) with the aim to reduce the cost of solar cell production [11]. Over the last decade the organic solar cell (OSC) became a popular research topic and between 2000 and 2007 publications on organic solar cells increased. The power conversion efficiency of the OSCs reaches nearly an average of 10% [12]. OSC reached the third generation photovoltaic (PV) technologies that contains the photo-active layer organic semiconductor [12]. Organic semiconductors has advantages over the traditional silicon based solar cell which are the low cost of fabrication, the ease of device processing such as the spin-coating or doctor blade techniques as well as the flexibility and lightweight of the substrates [13].

Chapter 2

Organic semiconductors

The study of organic semiconductor has been existing since 1940. Organic semiconductors are carbon based molecules with molecular structure containing sp^2 hybridized carbon atoms [14]. They are known as π conjugated molecules which have alternate single and double bonds. Electronic interactions for p_z orbitals on neighboring carbon atoms forms a π electronic system, with delocalized orbitals over conjugated segments in a size of a nanometer (see figure (2.1)).

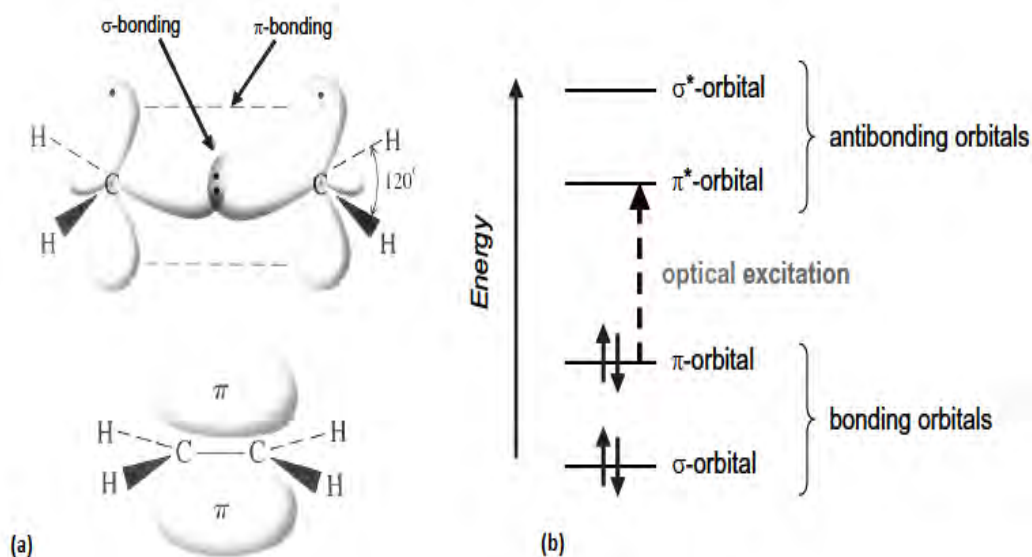


Figure 2.1: (a) Simplest π -conjugated electron system (where σ and π bonds are shown for ethylene), (b) depicts π -conjugated molecules energy level [1].

Oligomers are molecules formed with few number of monomer units unlike the polymers which are composed of several monomers. As the result oligomers have lower molecules

weight than the polymers. π -conjugated organic molecules are capable of charge transportation and they interact efficiently with light similar to inorganic materials, therefore, these systems can act as semiconductors in opto-electronic devices [15]. Charges can be created optically or electrically and because of delocalized π orbitals they would be free to move along and between molecules in a hopping process. Better understanding of charge transport in organic molecules resulted in realization of new classes of conjugated materials with enhanced properties of semiconductor. The first industrial application of organic semiconductors was in xerography and that is where photoconductive properties was exploited [15]. Application of organic semiconductors has emerged as an alternative to replace inorganic semiconductors due to their potential of being used to produce cheap photonic, electronic devices and also photovoltaic devices. However, organic materials used in fabrication of photovoltaic devices must possess a very good chemical stability and a great optical absorption in the visible range [16]. Organic compounds application found in electronic components include efficient organic light-emitting diodes (OLED's), organic field-effect transistors (OFET's), and organic solar cells (OSC's) [15].

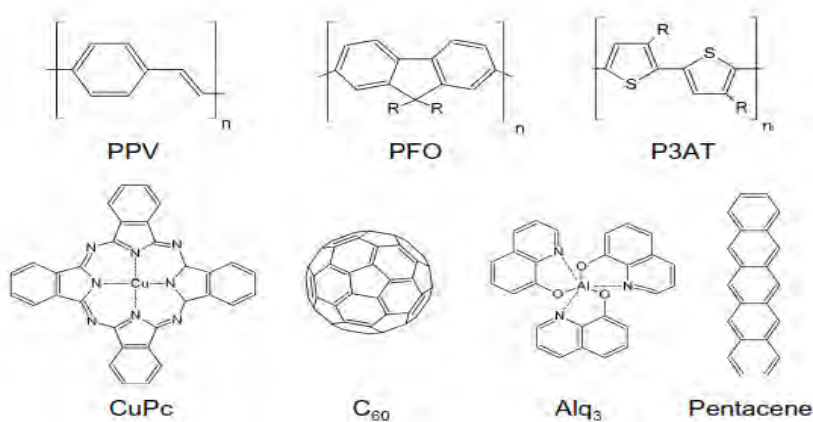


Figure 2.2: Organic semiconductors molecular structure [1].

2.1 The general properties of organic semiconductor

Organic semiconductors are composed of organic molecules which has gained a lot of attention for many applications such as in light-emitting diodes, switching devices and solar energy conversion. The use of organic semiconductors over inorganic materials gives advantages such as low cost device manufacturing, simple processing, easy control of physical properties of materials and also gives versatility in molecular design. In this sense, several organic semiconducting devices have been developed over decades ago including OLED's, OSC's, organic bistable memory devices and organic thin film transistors. However, the main focus for many researchers has been on studying the OLED's and OSC's devices. Organic semiconductors can be processed to form thin films with a large area. Thin film organic semiconductors can be produced on flexible substrates that gives them even more advantage to be used as the active components on efficient LED's, solar cells and other electronic devices [17]. Organic electronic devices is a growing field and organic films application in electro-photography have been the priority to researchers studying the interface of organic semiconductors. Organic materials play an important role in high performance polymer LED's because of the effectiveness on injection of charge and transport in thin films. Therefore, researchers focus has been on charge transport process limiting the current across the device and for that reason, a number of electrons and holes becomes available for radiative recombination [17]. The most common device structure of OSC in bulk heterojunction design is shown in figure (2.3). Organic semiconductors application in OSC's is facing a huge challenge because the large exciton binding energy does not allow efficient exciton dissociation. To fix this a photo-induced charge transfer between an electron donor (Poly-phenylene-venylene (PPV)) and C_{60} as an electron acceptor must be used (see figure (2.2)) [1]. OSC's use bulk heterojunction concepts of mixing donor and acceptor in one single layer, also due to the limited exciton diffusion length of approximately 10 nm. Regardless of the huge progress made so far on OSC's, researchers are still experiencing huge problems on achieving adequate life-time under ambient laboratory conditions.

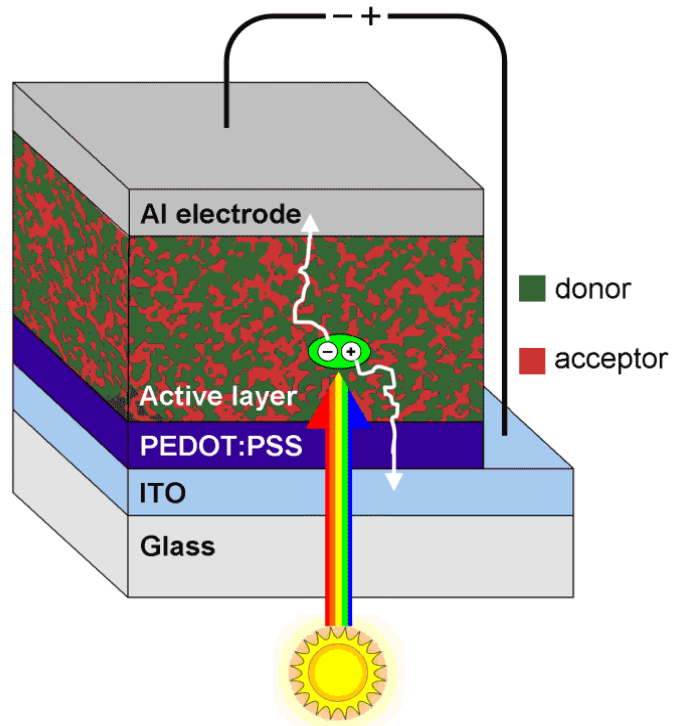


Figure 2.3: Organic solar cell (OSC) depicting the bulk heterojunction device [1].

Chapter 3

Charge transport properties

3.1 Charge transport theory

The charge transport across two oppositely charged electrodes has been the focus of intense investigation for the past several decades. From simple diode to the most complex electronic devices, charge transport across electrodes has been a very interesting phenomena for science as well as engineering [18]. The charge transport between electrodes has a significant influence on the performance of the devices and the earliest studies provided us with the spring board to look into this picture [18]. In 1938 a model was designed to understand the transport between two electrodes and the model was proposed to provide a picture on how an electron traverses between electrodes in semiconductor diodes [18].

3.2 Current Density Equation

The flow of charge mechanisms across a junction are drift and diffusion due to the applied electric field (E) and the gradient of charge concentration respectively (see figure (3.1)). The current equations based on the drift and charge diffusion theory in a device for positive and negative charges can be expressed as follows [19],

$$J_p = q\mu_p P(x)E - qD_p \frac{dP(x)}{dx}, \quad (3.1)$$

$$J_n = q\mu_n n(x)E + qD_n \frac{dn(x)}{dx}, \quad (3.2)$$

where E is the applied electric field in the x-direction, q is the elementary electronic charge, $n(x)$ -the electron density, D_p & D_n are the diffusion coefficients for positive &

negative charges, μ_p & μ_n are the mobilities for positive & negative charges and $P(x)$ is the probability. J_p & J_n are the current densities for positive and negative charges, respectively. The total conduction current can be expressed as,

$$J = J_p + J_n, \quad (3.3)$$

for the case where the current in the devices involves both types of charge carriers.

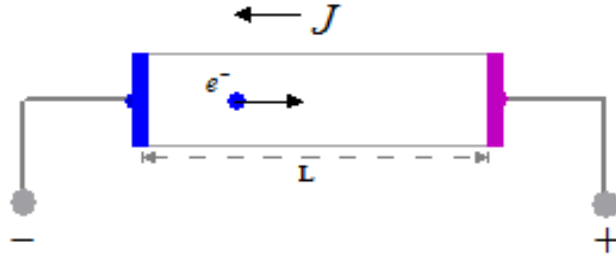


Figure 3.1: Schematic diagram representing two terminals of the voltage source across a device of thickness L [2].

3.3 Space charge-limited current

Space charge-limited regime between parallel electrodes is characterized by the fact that all traps are filled and the current reached steady state condition [20]. The current equation for single type of charge carrier and the Poisson equation can be used to deduce the current density equation which describes the steady state condition as,

$$\frac{dJ}{dx} = 0, \quad (3.4)$$

$$J = q\mu_n n(x)E(x), \quad (3.5)$$

$$\frac{dE}{dx} = \frac{q}{\epsilon} n(x), \quad (3.6)$$

where ϵ is the dielectric constant of the material and μ_n is the mobility. From the above equations (3.5) and (3.6) one can deduce,

$$\frac{dE}{dx} = \frac{J}{\epsilon\mu_n E(x)}, \quad (3.7)$$

and by definition $E = V/L$, then after re-arranging and solving the differential equation one finds the space charge-limited current in the absence of any traps which is the Mott-Gurney Law to be,

$$J = \frac{9}{8} \epsilon \mu_n \frac{V^2}{L^3}, \quad (3.8)$$

where V is the applied voltage and L is the distance between the electrodes. Current was assumed to be due to charge carriers of only one sign, reason being that diffusion effect was ignored and also the mobility was assumed to be field independent [19–21].

3.4 Thermionic emission and Field emission Theory

3.4.1 Thermionic emission theory

Thermionic emission may be referred as the electron emissions from a heated surface metal to any neighbouring medium. The well known example of thermionic emission is that about the electrons emission from hot cathode into a vacuum tube. However, the hot cathode may be a metal filament or a coated metal [17]. This process is very important in the operation of electric devices and can generate electricity. The temperature increase may cause the charge flow magnitude to increase. Therefore, if the metal is used as a cathode, then all the electrons emitted from the metal surface are collected at the anode of a vacuum diode, and the cathode is said to be in the saturation emission condition [17]. The current density (J) emitted is called the saturation current density (J_s). The Richardson equation relates the saturation current density (J_s) to the cathode's temperature and the work-function of the metal. The current density-voltage relation at low bias is usually linear up to a certain point because the electric field due to the injected carriers is ignored compared to that one due to the applied bias [17]. The slope of the $\ln(J)$ - V curve equals to 1 at the low electric fields, then that region is ohmic. The current density-voltage characteristics can be fitted using the model of Richardson-Schottky (RS) emission just above the ohmic region. However, the assumption of RS model based on the thermionic emission is that electrons from the metal can be injected into the polymer once the electrons obtained sufficient thermal energy to cross the maximum potential which resulted from the external superposition and image charge potential [17]. The RS model is valid at low fields as well as at high temperatures [17]. Therefore, at high fields, the metal work-function for thermionic emission is reduced, the Schottky barrier height is lowered

(image force lowering). Considering the image force lowering the Schottky equation can be written as,

$$J = A^* T^2 \exp\left(\frac{-\phi_B}{k_B T}\right) \exp\left[\sqrt{\frac{q^3 V}{4\pi\epsilon_0\epsilon_r d}} / k_B T\right], \quad (3.9)$$

where ϵ_0 , ϵ_r , d and ϕ_B are vacuum permittivity, optical dielectric constant, film thickness and the interface potential barrier height, respectively. k_B is the Boltzmann's constant, q is the elementary electronic charge, T the absolute temperature and V the applied voltage which is positive for the forward bias and negative for the reverse bias. A^* is the RS constant for free electrons which can be written as,

$$A^* = \frac{4\pi q m^* k_B^2}{h^3} = 120 A \text{ cm}^{-1} K, \quad (3.10)$$

where m^* is the effective charge carrier mass which equals that one of the free electron and h is the Planck's constant. Equation (2.9) may be re-written as,

$$\ln\left(\frac{J}{T^2}\right) = [-\phi_B + \left(\sqrt{\frac{q^3 V}{4\pi\epsilon_0\epsilon_r d}}\right) \frac{1}{k_B}] \frac{1}{T} + \ln(A^*). \quad (3.11)$$

From equation (3.11) plots of $\ln(J/T^2)$ versus $1000/T$ are straight lines at the given voltage (V), because all the other parameters are constant. The slope of equation (3.11) is called activation energy, and, the effective barrier height between the electrode and the film may be determined from the slope. The activation energy is defined as,

$$\phi_B = -\text{slope} + \left(\sqrt{\frac{q^3 V}{4\pi\epsilon_0\epsilon_r d}}\right) \frac{1}{k_B}. \quad (3.12)$$

3.4.2 Field emission theory: Background

Field emission well known as the emission of electrons from the conductors surface under the influence of a strong electrostatic field, as a result of the tunnel effect. Field emission neglects the charge image effect and also invokes the electron tunnelling from the metal through a triangular barrier into the continuum unbounded states; the process is called Fowler-Nordheim (FN) model for tunnelling injection. Electron emission from the surface with an applied electric field (E) has been employed over decades as a way to form high brightness sources. Since then, the surface properties of the emitter are crucial to the electron field emission, and extensive studies have described this solid-vacuum interface under the influence of an electric field (E). Fowler and Nordheim proposed a theory of field emission process based on tunneling phenomena from cold metals [22].

Fowler and Nordheim focused on the investigation of the electron emission from cold metal by means of strong external electric field, where they treated the electron emission as a quantum tunneling through a potential barrier [22]. Fowler and Nordheim evaluated the number of electrons $N_e(W)$ incident at a right angle on a surface of unit area per unit time with a kinetic energy W , according to Sommerfeld's theory [22]. They got,

$$N_e(W) = \frac{4\pi m \epsilon k T}{h^3} L\left(\frac{W - \mu}{kT}\right), \quad (3.13)$$

where,

$$L(\beta) = \int_0^\infty \frac{dy}{e^{\beta+y} + 1}, \quad (3.14)$$

and μ is the electron distribution parameter in the Fermi-Dirac statistics which is equivalent to the thermodynamic partial potential of an electron [22]. Hence the current (I) equation is given by,

$$I = \frac{4\pi m \epsilon k T}{h^3} \int_0^\infty D(W) L\left(\frac{W - \mu}{kT}\right) dW, \quad (3.15)$$

where ϵ is the electronic charge. With sufficient approximations involved it was easy to evaluate the current (I) equation and when inserting the numerical values for other constants, the current (I) equation became,

$$I = 6.2 \times 10^{-6} \frac{\mu^{\frac{1}{2}}}{(\chi + \mu)\chi^{\frac{1}{2}}} E^2 e^{-6.8 \times 10^7 \chi^{\frac{3}{2}}/E} Acm^{-2}, \quad (3.16)$$

where χ is the thermionic work-function. The temperature effect was neglected in the model, however, at ordinary temperatures is clear that the correction is very small [22]. The approximation of the limit $T = 0$ is valid for as long as μ/kT is very large, where μ and kT are 5 V and $8.6 \times 10^{-5} T$ respectively, which is adequate for all ordinary temperatures [22]. $\chi^{\frac{3}{2}} = 10$ for commonly used metals, also the exponential factor is said to be nearly $10^{-9} F^{-1}$ and that will be enough to make emission to be sensible for fields of magnitude greater than $10^7 Vcm^{-1}$ but emission would be very large for fields of the order $10^8 Vcm^{-1}$ [22].

It is not so easy to estimate the value of E , however, owing to the large effect of surface irregularities or peaks near where larger values of E were determined and there is a possibility of sensitive spots on the surface with a reduced value of χ [22]. Rother's

investigation verified that after a very careful preliminary heat treatment an electric field (E) as large as 10^7 Vcm^{-1} is required for extracting a reasonable current (I), that allows us to conclude that phenomenon of electron emission in intense electric fields is yet another phenomenon that can be accounted for in a satisfactory quantitative manner by Sommerfeld's theory [22]. The process of the FN model predicted that if the field emission dominates, then the J-V characteristics may be written as [17],

$$J = AE^2 \exp\left(\frac{-8\pi\sqrt{2m^*\phi_B^3}}{3hqE}\right), \quad (3.17)$$

where m^* is the effective charge carrier mass, E is the applied electric field, A in A/V^2) is a rate coefficient that contains a pre-factor for tunnelling and the rate back-flow [17]. Kao and Huang [17] deduced that the rate coefficient A can be expressed as,

$$A = \frac{q^3}{8\pi h\phi_B}, \quad (3.18)$$

Considering of the rate coefficient equation (3.18), the J-V characteristics may be given as,

$$J = AE^2 e^{\left(\frac{-K}{E}\right)}, \quad (3.19)$$

where,

$$K = \frac{8\pi\sqrt{2m^*\phi_B^3}}{3hq} = \text{constant}. \quad (3.20)$$

Equation (3.17) maybe re-written as follows after natural logarithms were introduced,

$$\ln\left(\frac{J}{E^2}\right) = -K\left(\frac{1}{E}\right) + \ln(A). \quad (3.21)$$

This is a straight line equation of $\ln(J/E^2)$ versus $(1/E)$ with a slope of $-K$ and the plot is called FN plot. Then the interface potential barrier height between the electrode and film may be determined from equation (3.10) since K is constant and can be expressed as,

$$\phi_B = \left[\frac{3Kqh}{8\pi\sqrt{2m^*}}\right]^{\frac{2}{3}}. \quad (3.22)$$

3.5 Injection limited current

The current becomes limited by injection when the average charge density in the sample approaches the charge density at the injecting contact. The injected current can no longer act as a reservoir but rather ceases to be ohmic, the current coming from such electrode will saturate at a sufficiently high voltage. However, very high electric fields can make some contact ohmic by causing a strong injection via tunnelling or other mechanism super-linear with electric field [23]. Although the average charge density in the samples is comparable to the charge density at the contact, but both of them should be much smaller than the capacitor charge related to unit volume [23]. Injection-limited current will only be observed for relatively low currents at high electric fields with materials possessing large values of dielectric permittivity and charge carrier diffusion, but often these features are met in thin organic films that are sandwiched between metals or semiconductors with moderate work-functions [23].

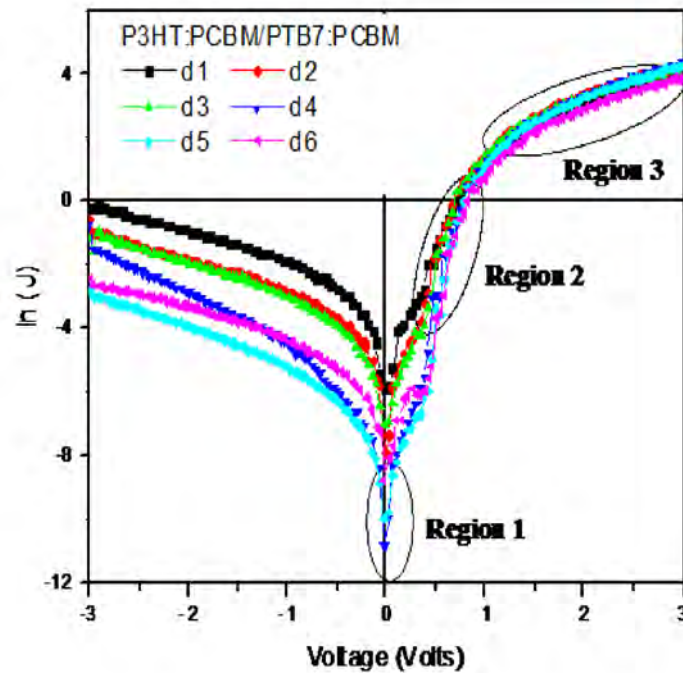


Figure 3.2: Dark current showing various transport phenomena [3].

Chapter 4

Characterization of a Solar Cell device

A solar cell is known for converting solar radiation into electric energy. A solar cell devices are fabricated by employing different processing techniques using a variety of materials. However, a solar cell has the potential of becoming an alternative renewable power source that is less expensive, flexible and accessible everywhere, provided that the power conversion efficiency (PCE) is increased. The current density-voltage characteristics of the solar cell diode obey a simple diode equation given by,

$$J = J_s(e^{qV/K_B T} - 1) - J_{ph}, \quad (4.1)$$

where V is the applied voltage, J_s and J_{ph} are the saturation and photo-generated currents, respectively. All the important parameters of the solar cell can be derived from the simple diode equation (4.1). The PCE is used to evaluate the solar cell performance and other parameters which are the fill-factor (FF), short-circuit current density (J_{sc}), open-circuit voltage (V_{oc}). The PCE of a solar cell can be defined as a number of electrons which leaves the device per unit time and per unit area over the number of photons incident per unit time per unit area [24]. The PCE can be determined by measuring the current density-voltage (J-V) characteristics under light conditions, where the photo-generated charge carriers in the cell are driven by the built-in electric field. Under illumination condition, when the applied voltage $V_a \gg \gg V_{oc}$, the cell is in forward biased condition, however, when $V_a \ll \ll V_{oc}$ it is reverse biased condition [24]. At some point on the J-V characteristics, the power unit area ($J \times V$) driven by the cell becomes the maximum power (P_{max}) that the cell can deliver to an external load. The power conversion efficiency

is the percentage of input power from light source that is converted to the output power at the operating point where the maximum power is produced by the device [25]. The power conversion efficiency (PCE) of a solar cell is given by,

$$PCE = \eta = \frac{P_{max}}{P_{in}} = FF \times \frac{J_{sc} \times V_{oc}}{P_{in}}, \quad (4.2)$$

and the ratio of P_{max} to the product of short-circuit current density (J_{sc}) and open-circuit voltage (V_{oc}) is called the fill-factor (FF) which also gives the shape of the J-V characteristics. FF is given by the following equation,

$$FF = \left| \frac{J_{max} \times V_{max}}{J_{sc} \times V_{oc}} \right|, \quad (4.3)$$

where $P_{max} = |J_{max} \times V_{max}|$ is the maximum power a device can produce, $P_{in} = 100 \text{ mWcm}^{-2}$ is the standard power input, J_{max} and V_{max} are the maximum current density and maximum voltage respectively. The other parameters are at the boundaries in J-V characteristics where power is produced by a device. Short-circuit current density (J_{sc}) is the current density when the applied voltage (V_a) across a device is zero and also the open-circuit voltage (V_{oc}) is the voltage when the current density in a device is zero [25]. P_{max} is the product of the maximum current density and maximum voltage where either the current or voltage is zero at both points. However, J_{sc} and V_{oc} act as J_{max} and V_{max} which are produced by device illumination. Figure (4.1) shows J-V characteristics of a solar cell under dark and illumination conditions. Under dark condition, there is no light meaning no current flowing through, up until the contacts starts injecting the charge carriers at the forward bias at voltage (V) greater than the V_{oc} . Under illumination condition, the short-circuit current density (J_{sc}) is the current measured when the applied voltage (V_a) across the solar cell is zero. The open-circuit voltage (V_{oc}) is the internal potential difference which neutralizes the current in the device [25].

4.1 Open-circuit voltage (V_{oc})

The total current density under illumination condition in a conventional silicon solar cell is given by [24],

$$J_{total} = J_0 \left(e^{\frac{qV}{nk_B T}} - 1 \right) - J_{ph}, \quad (4.4)$$

where n is the identity factor, J_0 is the reverse saturation current density under dark conditions and here J_{ph} equals to J_{sc} . From equation (4.4) above one can deduce the

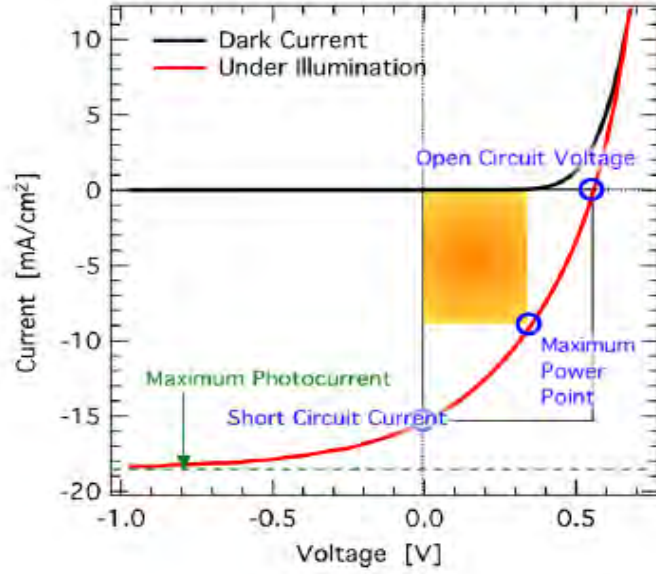


Figure 4.1: Typical J-V curve for bulk heterojunction organic solar cell device under both dark and illumination conditions [4].

open circuit voltage given by,

$$V_{oc} = \frac{E_{gap}}{q} + \frac{nk_B T}{q} \ln\left(\frac{J_{sc}}{J_s}\right), \quad (4.5)$$

where here J_{ph} does not equal to J_{sc} for the case of organic solar cell since it depends on the applied voltage V_a , and also the reverse saturation of dark current is not observed. The open-circuit voltage V_{oc} depends linearly on the energy difference E_{gap} between the highest occupied molecular orbit (HOMO) of the donor materials and the lowest unoccupied molecular orbit (LUMO) of the acceptor materials [24]. The study of Brabec et al. clearly shows the linear correlation between the first reduction potential and LUMO level of the fullerene acceptors. However, Gadisa et al. studies shows the changes in the V_{oc} with the variation of the first oxidation potential (HOMO level) of the donor conjugated polymer [26]. The study of Scharber et al. also showed the linear relation for many different bulk heterojunction solar cells between the oxidation potential (HOMO level) of the conjugated polymer and V_{oc} . The loss in charge carriers at the electrodes reduces the V_{oc} . V_{oc} is affected very easily by the nano-morphology of the active layer in the polymer fullerene bulk heterojunction solar cells. Ganzoring et al. study reported that in order to increase the V_{oc} in organic solar cells, one is required to modify the cathode by deposition of a thin layer of LiF between the metal electrode and organic semiconductor [26]. It is clear from equation (4.5) that any increase on energy difference E_{gap} or short-circuit current

density J_{sc} will result in an increase on V_{oc} , however, also a decrease on J_s will result on an increase of V_{oc} . To obtain the V_{oc} experimentally, current density (J) needs to be zero i.e. $V(J = 0) = V_{oc}$, this can be obtained from the J-V characteristics by reading the value of voltage (V) at $J = 0$ (see figure (4.1)).

Chapter 5

Organic Solar Cell (OSC)

Edmund Becquerel (1839) was the first physicist who discovered the photovoltaic effect. He observed the conversion of electromagnetic radiation into electricity. The first organic compound where photoconductivity was observed in solid anthracene (1906). The investigation on photovoltaic (PV) devices came in around 1950s, that is when a number of organic dyes, particularly chlorophyll and other related compounds, were studied [27]. Research dedicated on solar cells of less expensive type such as organic dyes and polymers has increased. However, the greatest thing about organic electronics is that once the physical requirements for applications is understood, chemists may manufacture mixtures with properties suited to opto-electronics applications. An organic solar cell (OSC), also known as plastic solar cell, it is a polymer solar cell type that uses organic electronics. OSC also uses a branch of electronics which deals with conductive organic polymers or small organic molecules for light absorption and charge transport to produce electricity by photovoltaic effect from sunlight [28]. Organic polymers and small organic molecules they both consist of conjugated systems. Conjugated systems is when carbon atoms covalently bond with another single and double bonds (the process of forming delocalized π bonding orbital with π^* anti-bonding orbital). The delocalized π orbital is the HOMO, while the π^* orbital is the LUMO. The excited state is created when organic materials absorb a photon. However, excited state would be considered as an electron-hole pair which is bound together by electrostatic interactions (exciton). The excitons are then broken up into free electron-hole pairs by effective fields. Effective fields break up excitons by causing the electron to fall from the conduction band of the absorber molecule into the conduction band of the acceptor molecule. Therefore, it is very important for

acceptor materials to always have lower conduction band edge than absorber materials. OSCs use the plastic which has low production costs in high volumes and are potentially cost-effective for photovoltaic applications.

5.1 Mechanism of charge generation in OSC

5.1.1 Light absorption

In most organic devices the absorbed light is very small when the band gap is very high. However, to absorb a 77% of solar radiation on earth, a 1.1 eV of bandgap is required, whereas most semiconducting polymers have bandgaps bigger than 2.0 eV which limits the absorption to be 30%. OSC photo-active layer is very small [13], with a thickness layer of 100 nm, which is required for exciton mobilities and low charge carrier. The absorption co-efficient of organic materials basically is higher compared to inorganic ones (silicon) [13]. The absorption spectrum of the organic photo-active layer must be identical to solar emission spectrum for the efficient collection of photons. In order to absorb more incident light, a thick enough photo-active layer is required. Organic materials optical absorption coefficient (α) is higher compared to crystalline silicon, however, for conjugated polymers (i.e. MDMO-PPV, P3HT, molecular dye, and zinc phthalocyanine (ZnPc)) α exceeds 10^5 cm^{-1} in the visible spectrum [29, 30]. The absorption co-efficient spectra of MDMO-PPV and P3HT lack absorption in red and near infrared region (NIR) part of the spectrum [29, 30]. Bandgap of 1.1 eV is optimum for PV device based on a single light absorbing medium. However, an increase in the photo-current is expected when decreasing the bandgap of organic materials and that makes it possible to harvest more sunlight, which is why researchers devoted themselves on obtaining organic polymers with an optical bandgap in the NIR [29, 30]. Even though increasing the thickness layer might be useful for light absorption but charge transport will suffer from high bulk resistance and that reduces the fill-factor (FF).

5.1.2 Exciton diffusion

All photo-excited excitons must ideally reach a dissociation site to create free charge carriers [28]. However such a site may be at the other end of the semiconductor, but their

diffusion length should be at least equal to the thickness layer, otherwise they recombine and photons are wasted. Exciton diffusion length usually ranges around 10 *nm* in polymer blends. Ideally, all excitons formed due to light absorption should lead to the formation of free charge carriers for an efficient organic solar cell. However, exciton transport is competing with other decay processes such as luminescence or radioactive recombination to the ground state [29, 30]. An exciton exponential lifetime (τ_{exc}) is determined by reciprocal value of all radiative and non-radiative decay rates together. Therefore, all excitons for an efficient solar cell have to reach the photo-active interface within τ_{exc} . However, the excitons transport occurs by diffusion and the distance an exciton is able to cross (L_{exc}) is [29, 30],

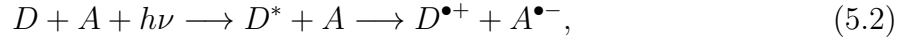
$$L_{exc} = \sqrt{D_{exc}\tau_{exc}}. \quad (5.1)$$

where D_{exc} is the excitons diffusion co-efficient. For polymer blends used in OSCs τ_{exc} is at most only several nanoseconds, and L_{exc} is limited to 10 *nm*. This implies that only those excitons formed within a distance of L_{exc} from the interface will contribute to charge separation. However, to avoid this problem, research has been devoted to increase the diffusion coefficient of excitons so that each generated exciton is always close to an interface between the donor and acceptor due to the offset of HOMO states of the donor and the acceptor [31].

5.1.3 Charge separation

Charge separation usually occurs at organic semiconductors or at the materials with enough difference between electron affinities (EA) and ionisation potentials (IA) [13]. However, one material acts as an electron acceptor (A) while the other act as an electron donor (D). If the difference is not adequate between EA and IA, then the exciton may jump onto the material with the lower band gap without separating the charges. However, this will recombine without contributing charges to the photo-current [13]. Charge creation is an important factor in converting solar radiations into electricity [28], however, photo-induced electron transfer in organic solar cell creates charges. Electrons moves from electron donor (D) material to electron acceptor (A) material with assistance from input energy ($h\nu$) of an absorbed photon [29, 30, 32]. Small EA are the molecular materials associated with D and high EA are associated with A. The required driving force is the difference between high and small electron affinities for exciton dissociation. In the process

of photo-induced electron transfer an exciton at the D/A interface decays by creation of the charge-separated state consisting of the radical cation of the donor ($D^{\bullet+}$) and the radical anion of the acceptor ($A^{\bullet-}$) [28–30, 32].



It is essential for an efficient charge generation that the charge-separated state is the thermodynamically and kinetically most favourite pathway for the exciton. However, it is important that the energy of the absorbed photon is used for the generation of charge-separated state and is not lost via competitive process like fluorescence or non-radiative decay [31]. Moreover, the charge-separated state must be stabilized so that photo-generated charges can migrate to one of the electrodes, therefore, the recombination or the back electron transfer should be slowed down as much as possible [29, 30]. In a homojunction between a p-n type silicon semiconductor under illumination electrons flow from the p-type to n-type semiconductor. However in a heterojunction based on an electron donor layer D and electron accepting layer A, under illumination electrons flow from the D to the A layer. The D layer is denoted as the p-type layer while the A layer as the n-type in analogy with a silicon p-n junction, however, p-type are the molecular materials that have a low IA and n-type are those having high EA [29, 30].

5.1.4 Charge transport in organic solar cell

Recombination is the process that affects charge transport during the journey towards the electrodes, specifically, if excitons do not reach the interface between the donor and acceptor [13]. However, the current might be limited because atoms or charges interactions may slow down the speed travel. Mechanisms of charge transport operating in OSC and inorganic solar cell (ISC) to drive charge carriers towards the electrodes are not identical. Absorption of light in ISC leads to electrons and holes generation in one material. However, the charge carriers have equal gradient concentration and spatial distribution, which is a driving force for the transport by the identical diffusion [29, 30]. Charge carriers are forced to move in one direction. However, that driven force in ISC is very small, and the electrical potential gradient present at the interface of a p-n junction will split the photo-induced electrons from the holes effectively [29, 30]. After charge transfer in OSC the electrons and holes are very close to each other, also there is a large gradient

of chemical potential which is driving the charge carriers away from exciton dissociating center. An electric field is the main driving force for charge transport in ISC, yet in OSC it is very unclear as to what extent will the internal electrical field contribute to charge transport. However, this is due to the differences in charge mobilities in organic molecules and inorganic semiconductors. The charge carriers velocity under the influence of the electric field (E) is given by [29, 30]:

$$v_{di} = \mu_i E, \quad (5.3)$$

where μ_i is the mobility. In molecular materials the mobility is small (less than $0.1 \text{ cm}^2/Vs$) as compared to inorganic semiconductors ($10^2 - 10^3 \text{ cm}^2/Vs$) [29, 30]. However, it is not clear yet if and how an electrostatic potential is formed in an organic bilayer, also due to the fact that molecular materials only contain low densities of mobile charge carriers. The kinetics rate for the various charge carrier recombination processes are important parameters in particular for organic solar cells, however, the process should be sufficiently slow to allow the charge carriers to reach the electrodes [29, 30].

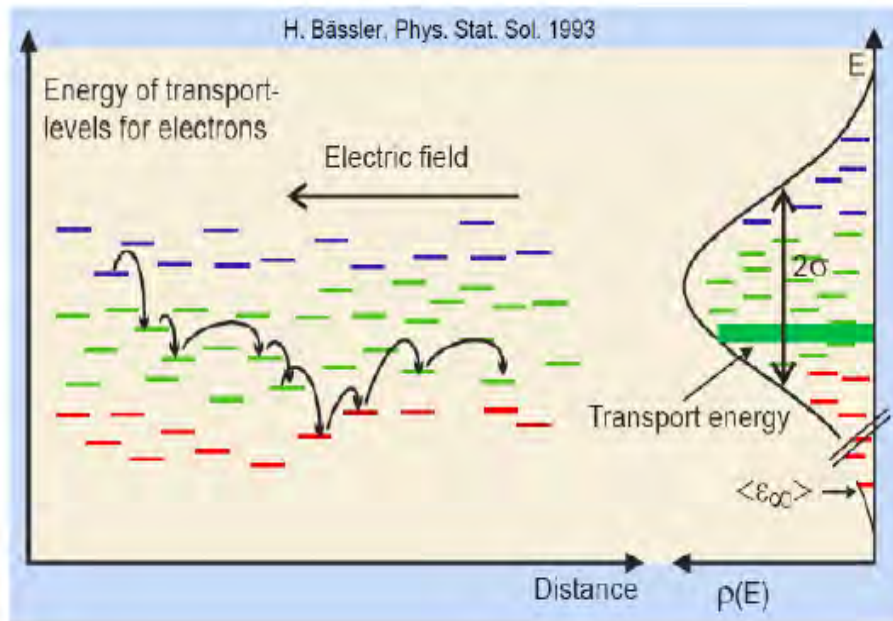


Figure 5.1: Charge transport by hopping between localised states with a gaussian energy distribution and disordered system of polymer medium [5].

5.1.5 Charge collection

The charges have to overcome the potential barrier of thin oxide layer in order to enter an electrode material with a relatively low work-function (Al or Ca), however, the metal may have formed a blocking contact with the semiconductor so that they do not reach the metal efficiently. Charge carriers collection is accomplished by a transparent conductive oxide (TCO) at the electrodes such as indium tin oxide (ITO) or $SnO_2 : F$ on one side and a metal contact on the other side [28]. The Ohmic contact that is formed between the electrodes and molecular layers need to be taken care of, however, special contact layers have been developed to obtain a better performance of the solar cell [28]. The contact layers examples are a PEDOT:PSS layer which is a charged conducting polymer layer at the ITO side and LiF layers at the metal contact, although it is unclear on how these layers improve the cell [31].

5.2 Organic Solar Cell (OSC) Device Architecture

A number of different device architecture have been developed in order to assist efficient photon to charge conversion. Separation of charge occurs between the two layers at the interface. Donor material must be in contact with higher work-function (ITO) electrode while the acceptor material with the lower work-function electrode (Al). However, single layer, bilayer and bulk heterojunction devices are different device architectures which are going to be discussed next.

5.2.1 Single layer device

The single layer device structure of OSC is comprised of a thin layer of conducting polymer sandwich between transparent electrode (ITO) and aluminium. R. N. Marks et al. (1994) created this structure by using 50-320 nm thickness of poly-phenylene-vinylene (PPV) sandwiched between an ITO and a low work-function cathode [33]. Under the intensity of $0.1 mW/cm^2$ quantum efficiencies of 0.1% for this device was reported. The low quantum efficiency resulted from intrinsically low mobility of charges through semiconducting organic materials and inefficient exciton separation [33, 34]. The carrier mobility of organic semiconductor is of the order of $10^{-3} cm^2/Vs$, while the mobility of a single crystalline silicon is of the order of $10^3 cm^2/Vs$. This indicates that the photo-generated charges

in semiconducting organic materials require more time to be collected from electrodes [33]. The OSC device efficiency is decreased by the slow charge transport, however, it also increases the chance of charge recombination in the device. The low PCE of OSC device is caused by exciton formation, which are strongly bound dipole charges of photo-excited semiconducting organics [33]. The bound exciton requires an additional exciton dissociation step to make free carriers, because the free electrons and holes are desired as an efficient charge carrier which can decrease the carrier generation efficiency. In a single layer OSC device, there is only one place to dissociate excitons into free carriers that is the interface between photo-active layer and a cathode [33]. It was known later that the excitons are more efficiently dissociated at the interface between donor and acceptor, and that how a bilayer OSC device can be developed by inserting an acceptor layer between a donor organic semiconductor and a cathode [33].

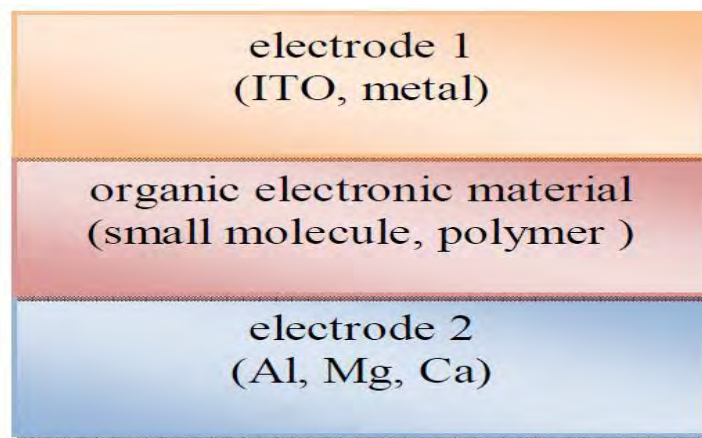


Figure 5.2: Configurations of single layer device [6].

5.2.2 Bilayer device

The phenomenon of exciton recombination and poor carrier transport in OSC device has been observed in pure films of non-polymeric organic semiconductors [35]. In a bilayer device the p-n type semiconductors are stacked on top of each other. The bilayer device was discovered by using many different materials combinations of organic semiconductor. The bilayer OSC device structure includes an additional electron transporting layer that

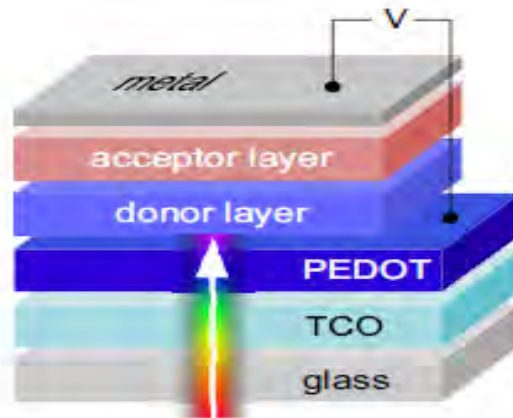


Figure 5.3: Configurations of bilayer device with planar heterojunction [4].

is found in the single layer OSC structure [33]. C. W. Tang (1985) improved the structure of OSC device which comprised of the pure films of non-polymeric organic semiconductor [29, 30, 35, 36]. However, he realized that, by making bilayer OSC device with organic semiconductors having the offset energy bands, then he noticed that the external quantum efficiency of OSC device could be improved to 15% at the wavelength of maximum absorption [35]. Bilayer device with thickness of 70 nm are made from copper phthalocyanine (as electron donor) and perylene tetracarboxylic derivative (as electron acceptor) [29, 30]. Tang put the photo-active material in different electrodes, where ITO was for positively charge collection and silver (Ag) for negatively charged collection [13, 33, 35]. However, a 1% of power conversion efficiency was obtained under simulated AM2 illumination (691 W/m^2) [29, 30, 33, 36, 37].

However, the bilayer OSC device PCE is still reported to be lower compared with the

inorganic devices. This happens because of the shortage of intrinsic exciton diffusion length in organic semiconductors, which is between 10-20 *nm*, however, researchers attempted to overcome this limitation in the bilayer OSC device by using buckminster fullerene, C_{60} in which the exciton diffusion length is around 20 *nm* [33, 36]. P. Peumans et al. replaced perylene tetracarboxylic derivative with C_{60} as an acceptor in the device structure and the device produced a PCE of 3.5% [33, 37]. Therefore, this improved PCE is caused by the longer distance travelled by excitons in the triplet state of C_{60} . The thickness of the acceptor and donor layers ranges between 40-60 *nm*, which is why the absorbed large amount of photon energy is not converted to free carriers and dissipated by recombination. Therefore, this indicates that photo-generated excitons are dissociated near the interface between donor and acceptor species [33]. Conjugated polymers is the other approach to build bilayer OSC device, however, Sariciftci et al. [33] fabricated the first bilayer OSC device to use conjugated polymer where the hole transports material was Poly[2-methoxy-5-(2'-ethyl-hexyloxy)-1,4-phenylene-vinylene] (MEH-PPV) and the electron transports material was C_{60} . Therefore, MEH-PPV played a huge part in photon absorption and transporting holes to anode, and C_{60} transports electrons to cathode. The bilayer device PCE of 0.04% obtained under monochromatic light incident of 514.5 *nm* improved the device performance compared to single layer device. Halls et al. optimized the conjugated polymers thickness and layer of C_{60} , then achieved a 9% of quantum efficiency under the intensity of 0.25 *mW/cm²* [33].

5.2.3 Bulk heterojunction (BHJ) device

The bulk heterojunction (BHJ) organic solar cell device is a thin film comprised of a mixture of donor and acceptor materials that are sandwiched between a pair of asymmetric electrodes. The donor material (i.e. polymer or small molecules) forms a hole-transporting path to the anode, while the acceptor material (i.e. fullerenes or inorganic material) forms the electron-transporting path to the cathode. Conjugated donor materials absorb light and are transformed into an excited state to produce bound electron-hole pairs or excitons [38]. Therefore, the excitons will diffuse between the domains of the donor and acceptor materials. However, the excitons will also dissociate to form positive and negative charge carriers due to the offset of energy level at the interface. After dissociation, the charge carriers are transported through the bi-continuous donor and acceptor pathways to their

respective electrodes [38]. With the efficient photo-induced electron transfer achieved from conjugated polymer to the fullerene discovery, then bulk heterojunction (BHJ) organic solar cell have become the most successful device structure that has been developed in the field (see figure (5.4)) to obtain self-assembling inter-penetrating network using various techniques such as spin-coating, doctor blading, inkjet and screen printing. OSC based on the bulk heterojunction concepts are a promising alternative for traditional silicon-based solar cell [39].

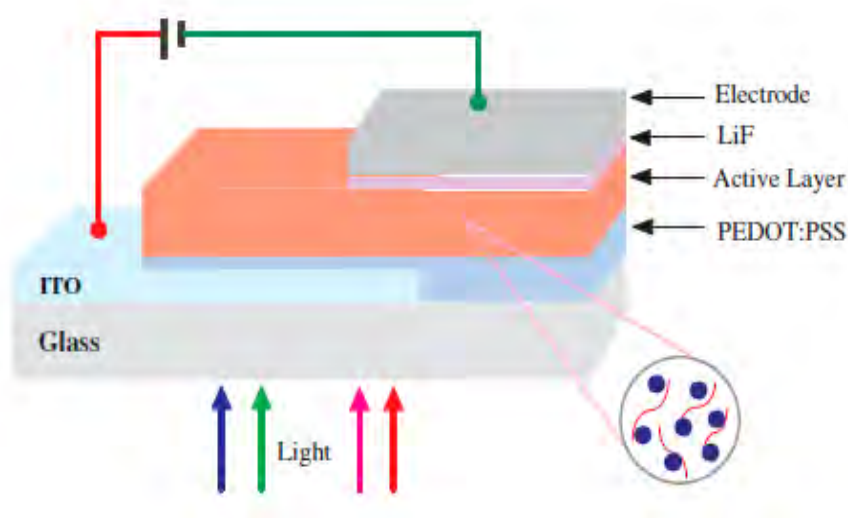


Figure 5.4: Configurations of bulk heterojunction organic solar cell device [7].

The bulk heterojunction is currently the most efficient device structure of organic solar cells. In this structure the interface between two different components is randomly distributed on the active layer, compared to the classical (bilayer) junction [30]. Morphological control is to make sure that electron and holes transport do occur at the collecting electrodes, however, it not necessarily for large interface charge-generation and to put an end on exciton loss [30, 40]. Electrical current densities are limited by incomplete utilisation of light incident due to a poor match of the absorption spectrum active layer with the solar spectrum and also organic semiconductors low charge carrier mobility. P3HT can be used because it has a high charge carrier mobility and reduced band gap compared to MDMO-PPV, however, in solar cells it has been used combined with PCBM [30, 41]. P3HT:PCBM mixtures power conversion efficiency compared to MDMO-PPV is increased, however, post-production treatment was used to achieve the higher efficiencies. After spin-

coating the active layer and deposition of the aluminium top electrode, P3HT:PCBM solar cell was treated by applying a higher voltage than the V_{oc} , and a temperature higher than the glass transition temperature of approximately 120°C led to much better efficiencies [30]. Post-production treatment would enhance the crystallinity of P3HT and improves charge carrier mobility. Power conversion efficiency of 5% was reported on devices made from P3HT:PCBM blend [13, 30].

Advantages of BHJ solar cell

The advantages of BHJ is that excitons can be dissociated anywhere in the active layer where there exists p-n type molecular interfaces. The interface distance should be in the order of the exciton diffusion length. Although absorption coefficient is very high (exceeding 10^5 cm^{-1}), a 20 nm double layer of donor and acceptor materials would not be optical dense, meaning large amount of photons would not be passing freely [30]. However, this can be fixed by combining p-n type materials, where it creates junctions throughout bulk materials and ensures that photo-generated exciton regardless of the thickness layer [30]. Materials that were firstly utilized in bulk heterojunction principle were fullerenes (with acronym PCBM) and MDMO-PPV [31]. Therefore, photo-generated charges should be able to cross to the collecting electrodes through those composite materials. The p-and-n type semiconductor materials are transported by holes and electrons, however, these materials should be mixed into a bi-continuous inter-penetrating network [30].

New development on OSC device

As we discussed the OSC above, the performance enhancement of an OSC device can be achieved effectively by using some strategies to maximize each step. Absorption of light may be made better by tuning band gap of organic semiconductors. Exciton diffusion may become better by making the area between donor and acceptor interface very large, however, organic semiconductors charge mobility affects the efficiency of charge transport [42]. The OSC device new development has exhibited the power conversion efficiency from 3% to 9% recently [43].

Chapter 6

Experimental

6.1 Sample Preparation

We used the ITO-coated glass as a substrate for the preparation of OSC device. The first step was to remove partially the ITO from the substrate surface by protecting half of the ITO-coated glass using the photo-resist. We then etched the unprotected part with acid solution containing 48% HCl : 48% H_2O : 4% NH_3 . After etching, samples were thoroughly cleaned successively with running tap water and were sonicated with detergent, distilled water, acetone and also with isopropanol for 10 minutes holding time in each solution, respectively. Then the samples were dried in the oven at 120°C temperature for 30 minutes. Once the samples were dried out, the PEDOT:PSS thin layer was spin-coated on the ITO side of the substrates at the speed of 3520 *rpm* for 40 seconds (see figure (6.1)). However, samples were instantly baked in the oven again at 120°C for 30 minutes. The binary and ternary molecules blend solutions were prepared separately in the chloroform solvent from the mixture of (P3HT:PCBM), (PTB7:PCBM), (P3HT:PCBM/PTB7:PCBM), and (PTB7:PCBM/P3HT:PCBM) (see figure (6.2)). In this experiment the concentration of solution used was 20 *mg/ml*, in all cases, the donor to acceptor weight ratio kept at a constant 1:1 and 1:1.5 for (P3HT:PCBM) and (PTB7:PCBM), respectively. The solution was sonicated at 40°C for 3 hours to enable homogeneity and inter-dispersion of the molecules. The active layers from the solution blends were spin-coated on a dried thin layer of PEDOT:PSS at the spin rate of 1200 *rpm* for 40 seconds. The samples were immediately transferred into the vacuum deposition chamber unit (see figure (6.3)) to deposit lithium fluoride (LiF) and aluminium (Al) electrodes. The vacuum deposition

chamber was pumped down to a pressure of 1×10^{-6} mbar. Thin LiF layer of 0.5 nm was deposited onto the active layers by evaporation, followed by the deposition of 60 nm thick Al layer. Device preparations were accomplished under ambient laboratory conditions with no use of glove box or clean room, except for depositing LiF and Al electrodes. The electrical properties of the samples were measured using the Keithely 2400 source meter under AM 1.5 solar simulator for 100 mW/cm^2 of integrated power intensity.



Figure 6.1: PI-KEM LTD Spin-Coater KW-4A used to spin-coat photo-active layers on the samples.

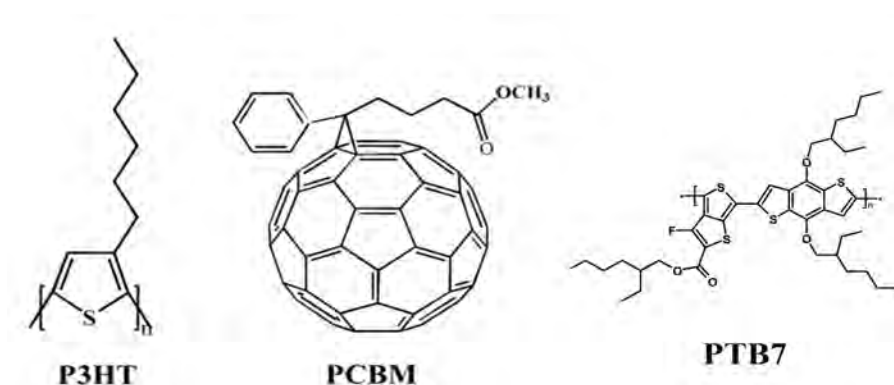




Figure 6.3: Edward Auto 306 vacuum deposition chamber unit used to deposit LiF and Al on the samples.

Chapter 7

Results and Discussion

7.1 Optical Absorption Properties

The UV-vis double beam spectrometer (T 80-PG-instruments Ltd.) model was used to collect data for UV-vis absorption and transmittance spectra from polymers blend thin films. The optical absorption properties measurements were conducted from thin films composed of PTB7:PCBM, PTB7:PCBM/P3HT:PCBM, P3HT:PCBM/PTB7:PCBM and P3HT:PCBM molecules blended at different stoichiometric ratios of PTB7 (1:1.5) and P3HT (1:1) (see Figure (7.1)) [8]. The optical absorption coefficient of organic molecules is very high, which can only mean that more light can be absorbed even in thin layer of materials [28]. OSCs have problems which are the low efficiency, low in stability as well as mechanical strength compared with inorganic photovoltaic cells. Moreover, organic semi-conducting materials have a large optical energy bandgap (E_g) compared to inorganic counterpart.

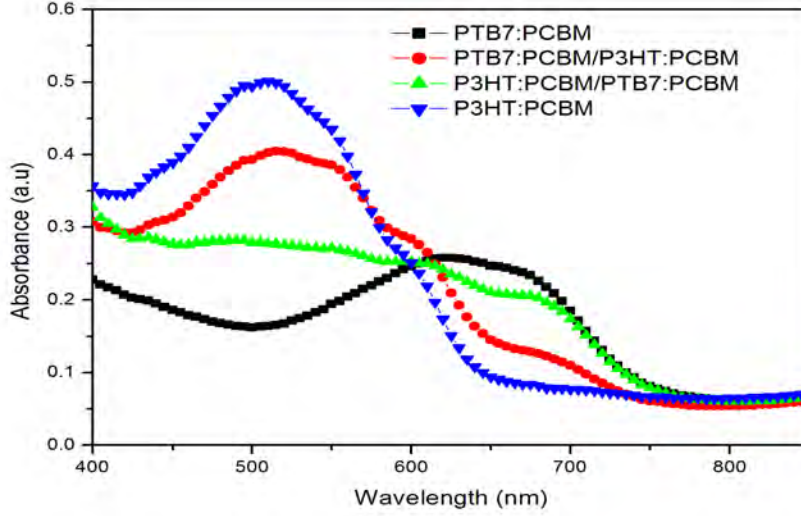


Figure 7.1: UV-Vis absorption spectra for all our experimental samples.

Figure (7.1) shows the UV-Vis absorption spectra taken from samples coated with binary molecules blend such as P3HT:PCBM and PTB7:PCBM. The other two spectra were taken from a double layer structure containing P3HT:PCBM as bottom layer and PTB7:PCBM as top layer denoted by (P3HT:PCBM/PTB7:PCBM). We also took spectrum from the structure (PTB7:PCBM/P3HT:PCBM). The optical absorption spectra of binary blends and double layers have an optical absorption in the visible region up to 770 nm. The spectrum of PTB7:PCBM and double layers have a wavelength of the optical absorption band edge of 775 nm compared to 650 nm of P3HT:PCBM, where is given extend to IR spectrum region. We used the wavelength of the on set for optical absorption to calculate energy bandgap (E_g) for our blends from the following equation,

$$E_g = h\nu = h\frac{c}{\lambda}, \quad (7.1)$$

where $h = 6.626 \times 10^{-34} J.s$ is the Plank's constant, $c = 2.998 \times 10^8 m/s$ is the speed of light in vacuum. Energy bandgaps of P3HT:PCBM, PTB7:PCBM and double layers were 1.7 eV, 1.6 eV and 1.6 eV respectively. We observed that bandgap of PTB7:PCBM and double layers is approximately the same which increases the optical absorption and in turn leads to the increased photons harvest. These energy bandgaps of binary blends are in good agreement with the one reported in the literature for the binary active layers [44].

7.2 Electrical properties

Several organic BHJ solar cells have been fabricated under ambient laboratory conditions at UKZN (Material science laboratory) in Pietermaritzburg campus. A BHJ layer of PTB7:PCBM and P3HT:PCBM were used as the photo-active layers, as well as double layers of PTB7:PCBM/P3HT:PCBM and P3HT:PCBM/PTB7:PCBM as the two photo-active layers. We employed a standard AM 1.5 (SS50AAA model) solar simulator for device illumination source. The Keithley 2400 source meter was used for the electrical measurements and the data were analysed by using the origin 6.1 software. After analysing the data one gets the important parameters of the solar cell i.e. (J_{sc}), (J_{max}), (V_{max}) and (V_{oc}). Once we have the J_{sc} , J_{max} , V_{max} and V_{oc} , then the PCE (η) and the fill-factor (FF) of the devices can be determined from equations (4.2) and (4.3), respectively. Figure (7.2) and (7.3) represent the J-V characteristics of the devices fabricated in the current investigation. Figure (7.2) was taken from samples under light illumination condition which clearly shows the power conversion ability of the device as depicted in the first quadrant of the figure.

The current-voltage characteristic of the devices is shown in figure (7.2) for both types of photo-active layers.

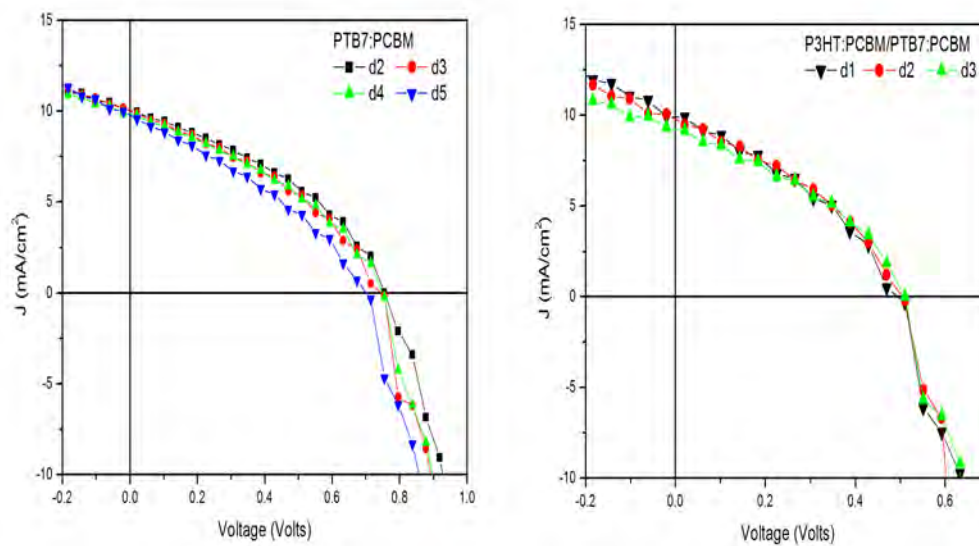


Figure 7.2: The J-V characteristics of BHJ OSC with photo-active layers of PTB7:PCBM and P3HT:PCBM/PTB7:PCBM blends. d1 to d5 represents the number of diodes on the device for both single and double layer.

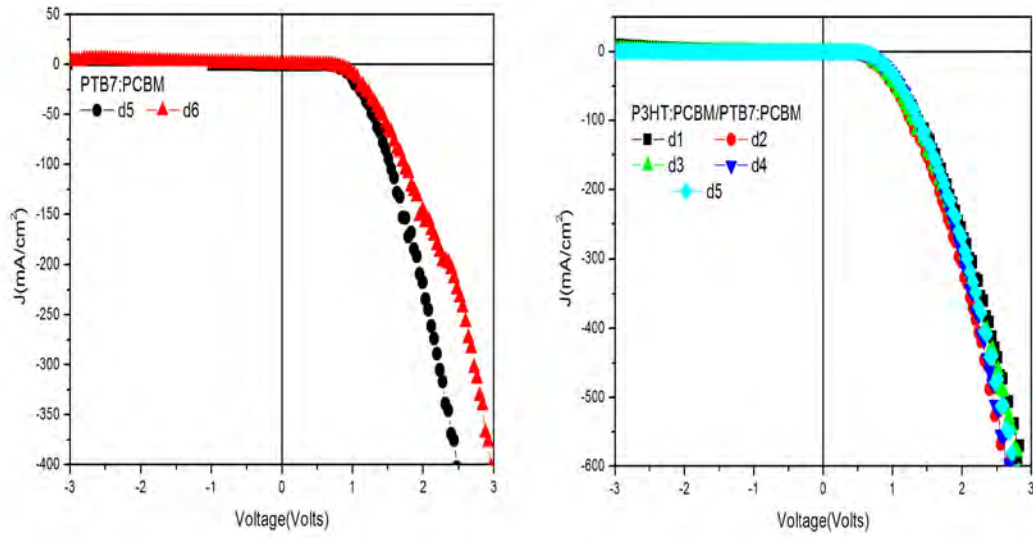


Figure 7.3: J-V curve under dark condition for both single and double layer.

The measured parameters of the better performing devices are given in tables (7.1) and (7.2) for both types of the photo-active layers under investigation.

See table (7.1) for our best performing device under illumination for single layer blend (PTB7:PCBM).

Diode	$V_{oc}(Volts)$	$J_{sc}(mAcm^{-2})$	$V_{MAX}(Volts)$	$J_{MAX}(mAcm^{-2})$	$FF(\%)$	$\eta(\%)$
2	0.7551	10.1180	0.4694	6.2650	38.5	2.94
3	0.7500	10.1900	0.4286	6.4047	35.9	2.75
4	0.7500	9.8992	0.4694	5.8863	37.2	2.76
5	0.7143	9.9877	0.4286	5.4321	32.6	2.33
6	0.7959	8.5097	0.5102	5.1408	38.7	2.62

Table 7.1: Best performing sample that was produced in the laboratory under illumination for (PTB7:PCBM) and the $P_{in} = 0.100 Wcm^{-2}$ and the $Area = 0.0657 cm^2$

See table (7.2) for our best performing device under illumination for double layer blend (P3HT:PCBM/PTB7:PCBM).

Diode	$V_{oc}(Volts)$	$J_{sc}(mAcm^{-2})$	$V_{MAX}(Volts)$	$J_{MAX}(mAcm^{-2})$	$FF(\%)$	$\eta(\%)$
1	0.5102	9.9051	0.2653	6.5304	38.3	1.73
2	0.5102	10.0679	0.3061	5.9232	35.3	1.81
3	0.5000	9.1655	0.3470	5.1617	39.1	1.79
4	0.5100	5.1051	0.3470	2.4750	33.0	0.86
5	0.5102	4.8298	0.3470	2.5517	35.9	0.89
6	0.5510	3.7156	0.3878	2.0646	39.1	0.80

Table 7.2: Best performing sample that was produced in the laboratory under illumination for (P3HT:PCBM/PTB7:PCBM) and the $P_{in} = 0.100 Wcm^{-2}$ and the $Area = 0.0957 cm^2$

The parameters from table (7.1) and (7.2) shows average values of V_{oc} , J_{sc} , FF and η for single layer device were calculated to be $V_{oc} = 0.75 V$, $J_{sc} = 9.74 mA/cm^2$, $FF = 36.6\%$ and $PCE = 2.7\%$, respectively. However, for a double layer device structure the average values are $V_{oc} = 0.52 V$, $J_{sc} = 7.13 mA/cm^2$, $FF = 36.8\%$ and $PCE = 1.3\%$, respectively. These values are in good agreement with the parameters reported in literature [8]. By looking at the power conversion efficiencies given above it is very clear that the PTB7:PCBM blend gives the better performing device compared to the P3HT:PCBM/PTB7:PCBM blend. The results shows that the presence of P3HT in the double layer structure dominated compared to PTB7 because of the higher density and that led to the low PCE which is attributed to the poor mixture of the two donor polymers in the photo-active medium.

7.3 Charge transport properties

The logarithm plot of the dark current ($\ln(J)$ - V) is given in Fig. (7.4) which represents a typical diode rectification behaviour. It clearly shows the different charge transport properties of the device. The figure (7.4) below is divided into 3 regions (1, 2 and 3), corresponding to three different charge transport properties.

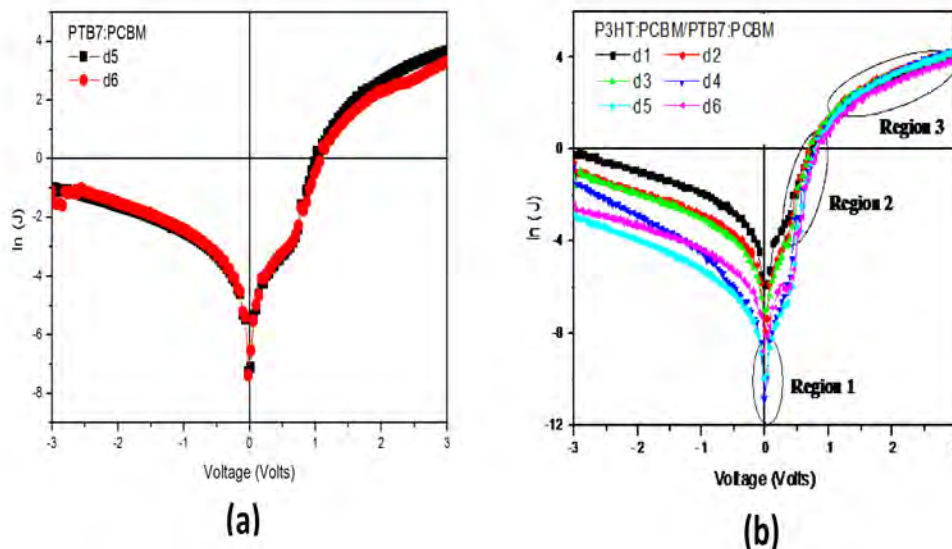


Figure 7.4: Schematic representation of $\ln(J)$ - V curve under dark condition, (a) is for binary molecular blend, (b) is for double layer molecular blend, where the behaviour on charge transport is the same for both (a) and (b).

On Region 1

We have a linear relation at the reversed bias voltage and low positive bias voltage till the point, where the E is neglected due to the injected carriers. This region has the Ohmic behaviour ($J \propto V$) because it obeys Ohm's Law.

$$J = qn\mu\frac{V}{d}, \quad (7.2)$$

On Region 2

We have the injection limited current region, where the electrical field is no longer negligible. However, the current due to the applied bias voltage increases exponentially ($J \propto e^{qV/kT}$) and the average charge carrier density on the device moves closely to charge density at the injecting contacts.

On Region 3

This is the space charge-limited current (SCLC) region, because the device inject much higher charge carrier densities over that of the applied bias voltages ($J \propto V^2$). SCLC would only occur where the transit time of any excess injected charge carriers are not more than that of bulk dielectric relaxation time. The space charge-limited current obeys Mott-Gurney Law equation, but that does not mean the traps are not there.

The modified Mott-Gurney Law equation is given by,

$$J = \frac{9}{8} \epsilon \epsilon_0 \mu_0 e^{\gamma \sqrt{\frac{V}{L}}} \frac{V^2}{L^3}, \quad (7.3)$$

The modified Mott-Gurney Law equation (7.3) above were fitted using the software called Origin 6.1 to calculate zero field mobility (μ_0) and the field activation factor (γ), but the field dependent mobility (μ) in the medium can be determined from the next equation which is written as,

$$\mu = \mu_0 e^{\gamma \sqrt{\frac{V}{L}}}, \quad (7.4)$$

(see tables (7.3) and (7.4)). The amount of the built-in potential from injection limited current to space charge-limited current used was $V_{bi} = 1.14 \text{ Volts}$. The thickness (L) of the active layer were $200 \times 10^{-9} \text{ m}$, the electric permittivity (ϵ) for polymers is between 3 and 5 (here we used 5) and for (ϵ_0) $8.854 \times 10^{-12} \text{ A}^2/\text{Fm}^2$ were used. The fitted results are in good agreement with the space charge-limited current theory from the literature (see figure (7.5) below) [45, 46].

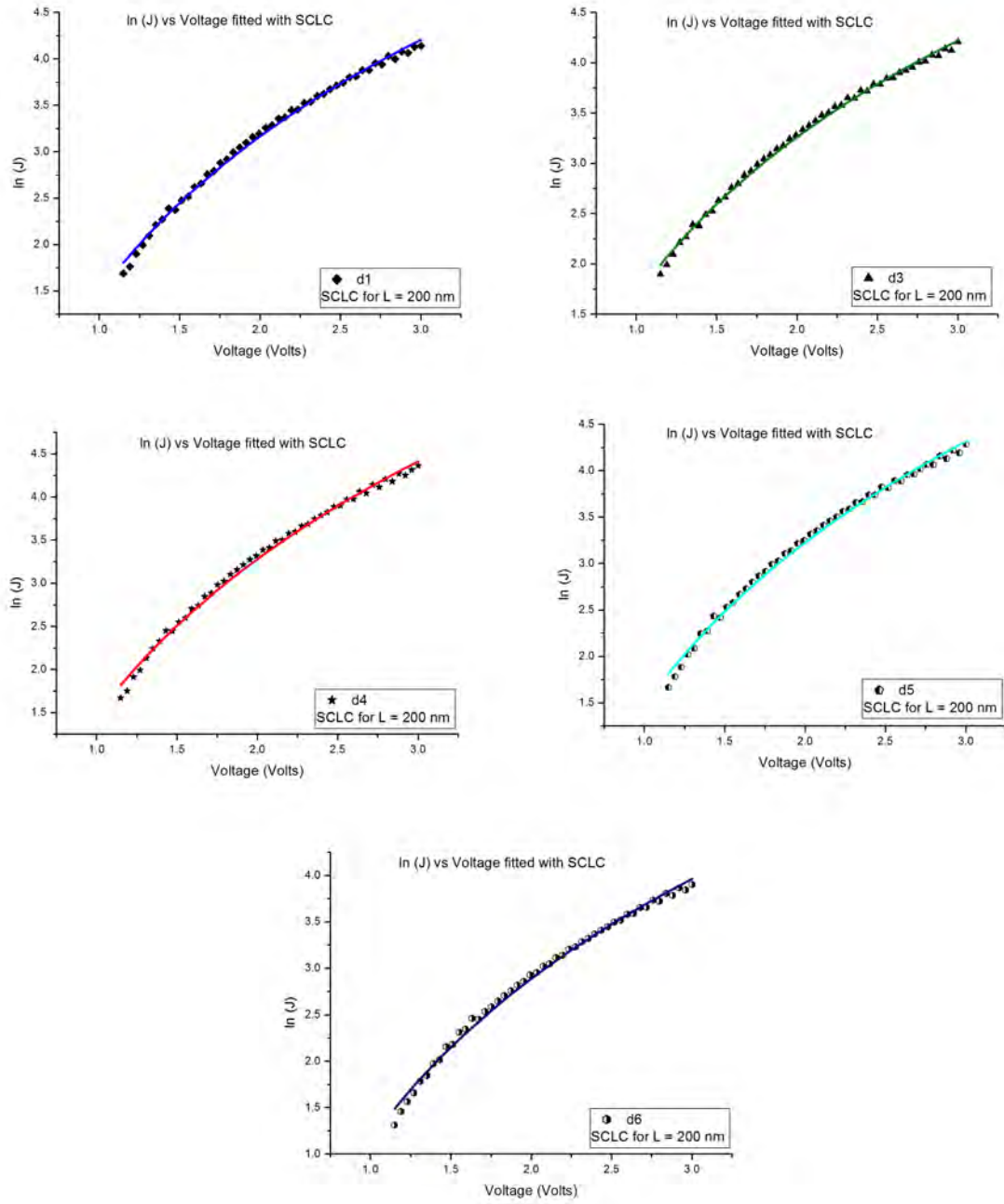


Figure 7.5: $\ln(J)$ vs Voltage fitted with space charge-limited current equation.

Below are the tables (7.3) and (7.4) showing the best dark current fitted results for both single and double layers in the space charge-limited current.

Diode	$\mu_0(cm^2/V.s)$	$\gamma(cm^{\frac{1}{2}}/V^{\frac{1}{2}})$	$\mu(cm^2/V.s)$
5	5.90×10^{-6}	7.60×10^{-3}	3.62×10^{-6}
6	6.81×10^{-6}	5.80×10^{-3}	2.72×10^{-6}

Table 7.3: Best fitted results for dark current single layer (PTB7:PCBM) in SCLC region 3.

Diode	$\mu_0(cm^2/V.s)$	$\gamma(cm^{\frac{1}{2}}/V^{\frac{1}{2}})$	$\mu(cm^2/V.s)$
1	3.39×10^{-6}	3.70×10^{-3}	8.21×10^{-6}
3	5.42×10^{-6}	2.40×10^{-3}	9.60×10^{-6}
4	2.52×10^{-6}	5.10×10^{-3}	8.52×10^{-6}
5	2.93×10^{-6}	4.40×10^{-3}	8.37×10^{-6}
6	2.20×10^{-6}	4.20×10^{-3}	5.98×10^{-6}

Table 7.4: Best fitted results for dark current double layer (P3HT:PCBM/PTB7:PCBM) in SCLC region 3.

The average mobilities of binary molecular blend (PTB7:PCBM) and double layer molecular blend (P3HT:PCBM/PTB7:PCBM) (see tables (7.3) and (7.4)) were both determined to be $3.17 \times 10^{-6} cm^2/Vs$ and $6.78 \times 10^{-6} cm^2/Vs$ for binary and double layer molecular blends, respectively. The measured average mobilities are found in the range reported in the literature [45, 46]. The zero field mobilities of the single layer found to be better than the double layer which consistent with device performance.

7.4 Morphology of P3HT:PCBM

The scanning electron microscope (SEM) was used on this project to study the surface morphology of the photo-active layers (P3HT:PCBM) generated by spin-coating on glass substrate. The use of SEM is common for surface characterization and many OSC researchers have shown interest on the top surface morphology of a spin-cast thin film, because it provides information about the surface topology as well as roughness [38]. The incident electrons interact within the sample and that causes back-scattered electrons or secondary electrons, which are identified to produce a clear picture. Figure (7.6) shows the surface morphology of the blended thin film molecules.

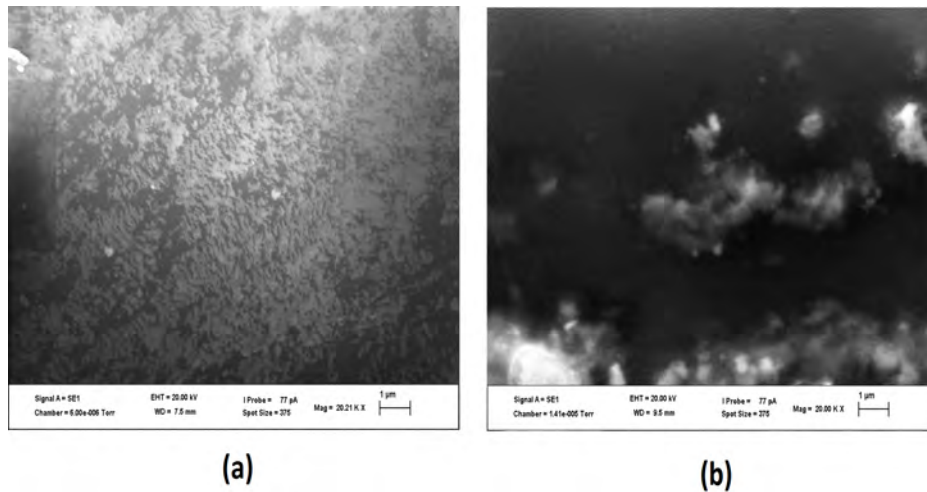


Figure 7.6: SEM image for photo-active layer of BHJ solar cell fabricated under laboratory ambient conditions.

On figure (7.6(a)) the shaded dark region or dark clusters are associated with P3HT. On figure (7.6(b)), the smoke like white shades or white large clusters are presumed to be PCBM, which is randomly distributed all over the P3HT medium and white large clusters prevent smooth charge transport. However, the random distribution of PCBM on P3HT medium increases the charge separation at the donor or acceptor interfaces. Researchers has reported that when blending P3HT with PCBM the morphology of the blends becomes more complicated and morphology can influence the performance of the device [38].

Chapter 8

Conclusion

Single and double layer bulk heterojunction organic solar cell comprised of P3HT:PCBM and PTB7:PCBM blends molecules as a photo-active layer with different structures (single binary layer and double layer blends) were studied in this dissertation under ambient laboratory conditions. The power conversion efficiencies (η), the fill-factor (FF), and other important parameters of the organic solar cell were determined from the J-V characteristics (see figure (4.1)). However, single binary layer blend consists of (PTB7:PCBM) was the best performing device in our experiments exhibiting the average power conversion efficiency (η) of 2.7% and FF of 36.6%, while double layer blend consisting of (P3HT:PCBM/PTB7:PCBM) produced the average power conversion efficiency (η) of 1.3% and FF of 36.8% (see tables (7.1) and (7.2), respectively). The glass substrate thorough cleaning and thermal annealing treatment gave a boost on enhancing the power conversion efficiency and the fill-factor, while that lowers the series resistance. However, the power conversion efficiencies that were determined in ambient laboratory condition when not using the glove box or clean room were expected. The morphology also played an important role in improving the solar cell power conversion efficiency, because P3HT:PCBM molecules blends adopt an organized morphology. Therefore, the absorption spectra will spread out then J_{sc} will increase, while V_{oc} is been reduced. The charge transport field dependent (μ) and zero field (μ_0) mobilities as well as the field activation factor (γ) were determined from the fitted data of $\ln(J)$ versus Voltage with the space charge-limited current equation (see figure (7.5) and tables (7.3) and (7.4)). The charge transport mobilities for organic materials can go as higher as $0.1 \text{ cm}^2/V.s$ and as lower as from 10^{-6} to $10^{-3} \text{ cm}^2/V.s$ [45, 46]. Therefore, in OSC, when the mobility is low then smaller current

would be generated. Mobilities on tables (7.3) and (7.4) are in the lowest range, then we can conclude that the analysis of charge transport properties were conducted successfully. However, success on this dissertation proves that organic solar cell has a potential to serve as alternative source of clean energy sources from the sun due to their ability for low cost solar energy harvesting and flexibility on applications. The project overall was fascinating and hard at the same time. In moving forward, we are going to use organic semiconductors to form the basis of the electronic components that are now increasingly used in smart phones, television sets and other devices, because they consume so little power. Inorganic semiconductors are going to be used as well.

Annexure

Below are the tables for measured parameters of the better performing devices under illumination for single & double layer blends for both types of the photo-active layers under the investigations.

Diode	$V_{oc}(Volts)$	$J_{sc}(mAcm^{-2})$	$V_{MAX}(Volts)$	$J_{MAX}(mAcm^{-2})$	$FF(\%)$	$\eta(\%)$
1	0.7959	9.7610	0.5510	5.1413	36.5	2.83
2	0.7959	6.9632	0.5102	4.3394	39.9	2.21
3	0.7959	9.8396	0.5102	5.8251	38.0	2.97
4	0.7551	9.4654	0.4694	5.8155	38.2	2.73

Table 8.1: Best performing sample that was produced in the laboratory under illumination for (PTB7:PCBM) after 30 minutes and the $P_{in} = 0.100 Wcm^{-2}$ and the $Area = 0.0657 cm^2$

Diode	$V_{oc}(Volts)$	$J_{sc}(mAcm^{-2})$	$V_{MAX}(Volts)$	$J_{MAX}(mAcm^{-2})$	$FF(\%)$	$\eta(\%)$
1	0.6327	3.2384	0.4286	1.7693	37.0	0.76
2	0.6341	3.5457	0.4286	2.0556	39.2	0.88
3	0.6327	3.6242	0.4694	1.9133	39.2	0.90
4	0.6327	3.9746	0.3470	2.5990	35.9	0.91
5	0.6300	2.0210	0.4286	1.1097	37.4	0.48
6	0.6327	1.9932	0.3878	1.2281	37.8	0.48

Table 8.2: Best performing sample that was produced in the laboratory under illumination for (PTB7:PCBM/P3HT:PCBM) and the $P_{in} = 0.100 Wcm^{-2}$ and the $Area = 0.1157 cm^2$

Diode	$V_{oc}(Volts)$	$J_{sc}(mAcm^{-2})$	$V_{MAX}(Volts)$	$J_{MAX}(mAcm^{-2})$	$FF(\%)$	$\eta(\%)$
1	0.6327	1.1929	0.4286	0.5839	33.2	0.25
2	0.5999	1.7562	0.3878	1.0762	39.6	0.42
4	0.5989	1.9920	0.4286	1.0755	38.6	0.46
5	0.6327	1.9496	0.4286	1.0442	36.3	0.45
6	0.5919	2.0714	0.3878	1.2454	39.4	0.48

Table 8.3: Best performing sample that was produced in the laboratory under illumination for (P3HT:PCBM/PTB7:PCBM) after 30 minutes and the $P_{in} = 0.100 Wcm^{-2}$ and the $Area = 0.0957 cm^2$

Diode	$V_{oc}(Volts)$	$J_{sc}(mAcm^{-2})$	$V_{MAX}(Volts)$	$J_{MAX}(mAcm^{-2})$	$FF(\%)$	$\eta(\%)$
1	0.4694	6.37552384	0.3061	3.6625	37.5	1.12
2	0.4694	5.9607	0.3061	3.3249	36.4	1.03
3	0.5102	5.2498	0.3061	3.4293	39.2	1.05
4	0.5510	4.7757	0.3061	3.0926	36.0	0.95
6	0.5510	3.6950	0.3470	2.2181	37.8	0.77

Table 8.4: Best performing sample that was produced in the laboratory under illumination for (P3HT:PCBM/PTB7:PCBM) and the $P_{in} = 0.100 Wcm^{-2}$ and the $Area = 0.0957 cm^2$

Diode	$V_{oc}(Volts)$	$J_{sc}(mAcm^{-2})$	$V_{MAX}(Volts)$	$J_{MAX}(mAcm^{-2})$	$FF(\%)$	$\eta(\%)$
1	0.5919	7.0642	0.3470	4.3906	36.4	1.52
2	0.5919	7.7432	0.3878	4.6368	39.2	1.80
3	0.5510	7.5499	0.3878	4.8023	44.8	1.86
4	0.5510	7.5726	0.3878	4.9076	45.6	1.90
5	0.5919	7.6280	0.3470	5.4295	41.7	1.88
6	0.5919	7.4460	0.2245	5.8784	29.9	1.32

Table 8.5: Best performing sample that was produced in the laboratory under illumination for (P3HT:PCBM) and the $P_{in} = 0.100 Wcm^{-2}$ and the $Area = 0.0657 cm^2$

Diode	$V_{oc}(Volts)$	$J_{sc}(mAcm^{-2})$	$V_{MAX}(Volts)$	$J_{MAX}(mAcm^{-2})$	$FF(\%)$	$\eta(\%)$
1	0.5510	6.6272	0.3470	3.9772	37.8	1.38
2	0.5919	7.5689	0.3878	4.6321	40.1	1.80
3	0.5919	7.5629	0.3878	4.7476	41.1	1.84
4	0.5919	7.4174	0.3470	5.3898	42.6	1.87
5	0.5510	7.7986	0.3878	4.4236	41.5	1.72
6	0.5510	8.0521	0.3878	5.2448	45.8	2.03

Table 8.6: Best performing sample that was produced in the laboratory under illumination for (P3HT:PCBM after 30 minutes) and the $P_{in} = 0.100 Wcm^{-2}$ and the $Area = 0.0657 cm^2$

Below are the tables showing the best dark current fitted results under dark conditions for both single & double layer blends in the space charge-limited current.

Diode	$\mu_0(cm^2/V.s)$	$\gamma(cm^{\frac{1}{2}}/V^{\frac{1}{2}})$	$\mu(cm^2/V.s)$
1	1.34×10^{-6}	5.50×10^{-3}	9.19×10^{-6}
2	5.31×10^{-6}	4.40×10^{-3}	2.48×10^{-6}
3	8.03×10^{-6}	4.10×10^{-3}	3.37×10^{-6}
4	8.80×10^{-6}	3.60×10^{-3}	3.10×10^{-6}
6	7.06×10^{-6}	1.70×10^{-3}	8.47×10^{-6}

Table 8.7: Best fitted results for dark current double layer blend (PTB7:PCBM/P3HT:PCBM) in SCLC region 3.

Diode	$\mu_0(cm^2/V.s)$	$\gamma(cm^{\frac{1}{2}}/V^{\frac{1}{2}})$	$\mu(cm^2/V.s)$
1	4.53×10^{-6}	2.00×10^{-3}	4.81×10^{-6}
2	4.67×10^{-6}	1.00×10^{-3}	4.83×10^{-6}
3	4.50×10^{-6}	1.30×10^{-3}	6.67×10^{-6}
4	4.80×10^{-6}	1.10×10^{-3}	6.71×10^{-6}
5	5.33×10^{-6}	4.00×10^{-3}	6.02×10^{-6}
6	3.08×10^{-6}	3.00×10^{-3}	3.38×10^{-6}

Table 8.8: Best fitted results for dark current single layer blend (P3HT:PCBM) in SCLC region 3.

Bibliography

- [1] W. Brütting. Organic semiconductors. *physica status solidi (a)*, 202(7):1–11, 2005.
- [2] J.T. Bell. *Preparation and Characterization of organic solar cells:MSc Dissertation*. UKZN, 2013.
- [3] A. Moliton and J.M. Nunzi. How to model the behaviour of organic photovoltaic cells. *Polymer International*, 55(6):583–600, 2006.
- [4] C. Deibel and V. Dyakonov. Polymer–fullerene bulk heterojunction solar cells. *Reports on Progress in Physics*, 73(9):096401, 2010.
- [5] H. Bässler and A. Köhler. Charge transport in organic semiconductors. In *Unimolecular and Supramolecular Electronics I*, pages 1–65. Springer, 2012.
- [6] S.M. Shauddin. Comparison among various emerging pv cells with history, current status and future challenges. *Energy and Power*, 3(6):91–105, 2013.
- [7] E.A.A. Arbab, B.A. Taleatu, and G.T. Mola. Environmental stability of ptb7: Pcbm bulk heterojunction solar cell. *Journal of Modern Optics*, 61(21):1749–1753, 2014.
- [8] E.A.A. Arbab, B.A. Taleatu, and G.T. Mola. Ternary molecules blend organic bulk heterojunction solar cell. *Materials Science in Semiconductor Processing*, 40:158–161, 2015.
- [9] A. Hammer, D. Heinemann, C. Hoyer, R. Kuhlemann, E. Lorenz, R. Müller, and H.G. Beyer. Solar energy assessment using remote sensing technologies. *Remote Sensing of Environment*, 86(3):423–432, 2003.
- [10] S.S. Sun and Z. Cheng. Organic and polymeric photovoltaic materials and devices. In *Introduction to Organic Electronic and Optoelectronic materials and devices*, pages 401–402. Taylor & Francis Group, 2008.

- [11] T. Manfred. Organic solar cells: Advantages, possibilities and limits of bulk hetero-junction solar cells. In *Sustainability Marketing and Innovation*. John Wiley & Sons, 2010.
- [12] C.J. Brabec, S. Gowrisanker, J.J.M. Halls, S. Laird, S. Jia, and S.P. Williams. Polymer–fullerene bulk-heterojunction solar cells. *Advanced Materials*, 22(34):3839–3856, 2010.
- [13] J.M. Nunzi. Organic photovoltaic materials and devices. *Comptes Rendus Physique*, 3(4):523–542, 2002.
- [14] J. Nelson. Polymer: fullerene bulk heterojunction solar cells. *Materials today*, 14(10):462–470, 2011.
- [15] S.S. Sun and L.R. Dalton. Molecular semiconductors. In *Introduction to Organic Electronic and Optoelectronic materials and devices*, pages 287–288. Taylor & Francis Group, 2008.
- [16] G. Horowitz. Organic semiconductors for new electronic devices. *Advanced Materials*, 2(6-7):287–292, 1990.
- [17] Z. Chiguvare, J. Parisi, and V. Dyakonov. Current limiting mechanisms in indium-tin-oxide/poly3-hexylthiophene/aluminum thin film devices. *Journal of Applied Physics*, 94(4):2440–2448, 2003.
- [18] K.S. Dieter. Semiconductor material and device characterization. In *Charge Transport properties*, pages 128–131. John Wiley & Sons, 2006.
- [19] S.M. Sze. *Semiconductor Devices:Physics and technology*. John Wiley & Sons, 2008.
- [20] P.N. Murgatroyd. Theory of space-charge-limited current enhanced by frenkel effect. *Journal of Physics D: Applied Physics*, 3(2):151, 1970.
- [21] N. Dasgupta and A. Dasgupta. *Semiconductor Devices:Modelling and Technology*. PHI Learning Pvt.Ltd, 2004.
- [22] R.H. Fowler and L L. Nordheim. Electron emission in intense electric fields. *Proceedings of the Royal Society of London. Series A, Containing Papers of a Mathematical and Physical Character*, pages 173–181, 1928.

- [23] S.S. Sun and L.R. Dalton. Introduction to organic electronic and optoelectronic materials and devices. In *Space charge limited current*, pages 380–381. Taylor & Francis Group, 2008.
- [24] P. Kumar and S. Chand. Recent progress and future aspects of organic solar cells. *Progress in Photovoltaics: Research and applications*, 20(4):377–415, 2012.
- [25] Keithley Instruments et al. Making i-v and c-v measurements on solar/photovoltaic cells using the model 4200-scs semiconductor characterization system. *Keithley Application Note Series*, (2876), 2007.
- [26] S. Günes, H. Neugebauer, and N.S. Sariciftci. Conjugated polymer-based organic solar cells. *Chemical reviews*, 107(4):1324–1338, 2007.
- [27] H. Spanggaard and F.C. Krebs. A brief history of the development of organic and polymeric photovoltaics. *Solar Energy Materials and Solar Cells*, 83(2):125–146, 2004.
- [28] S.V.D. Prasad, V. Krishnanaik, and K.R. Babu. Analysis of organic photovoltaic cell. *International Journal of Science and Modern Engineering (IJISME) ISSN*, pages 2319–6386.
- [29] T.J. Savenije. *Organic Solar Cells Coated*. PhD thesis, Delft ChemTech, Faculty of Applied Sciences. Delft University of Technology, 2009.
- [30] M. Kaushik and B. Kaushik. Organic solar cells: Design, synthesis and characterization. *International Journal of Engineering*, 2(7):310–319, 2013.
- [31] M. Kaushik and B. Kaushik. Organic solar cells: design, synthesis and characterization. *International Journal of Engineering Science, ISS2306-64742(7)*, 2013.
- [32] R. Janssen. Department of chemical engineering, chemistry and applied physics: eindhoven university of technology. *Solid State Physics, The Netherlands*, 2009.
- [33] M. Kim, M.G. Kang, L.J. Guo, and J. Kim. Understanding organic photovoltaic cells: Electrode. *Nanostructure, Reliability, and Performance*, 2009.
- [34] S.M. Sze. *Physics of Semiconductor devices*. John wiley & Sons, New York, 1981.

- [35] K.M. Coakley and M.D. McGehee. Conjugated polymer photovoltaic cells. *Chemistry of materials*, 16(23):4533–4542, 2004.
- [36] J. Roncali. Molecular bulk heterojunctions: an emerging approach to organic solar cells. *Accounts of chemical research*, 42(11):1719–1730, 2009.
- [37] M.V. Martinez-Diaz, G. de la Torre, and T. Torres. Lighting porphyrins and phthalocyanines for molecular photovoltaics. *Chemical Communications*, 46(38):7090–7108, 2010.
- [38] X. He, S. Mukherjee, S. Watkins, M. Chen, T. Qin, L. Thomsen, H. Ade, and C.R. McNeill. Influence of fluorination and molecular weight on the morphology and performance of ptb7: Pc71bm solar cells. *The Journal of Physical Chemistry C*, 118(19):9918–9929, 2014.
- [39] Chunfu Zhang, Dazheng Chen, Yue Hao, Zhenhua Lin, and Zhizhe Wang. *Investigation of Organic Bulk Heterojunction Solar Cells from Optical Aspect*. INTECH Open Access to Publisher, 2013.
- [40] O.A.O. Gassim. *Improvement of Performance of Conjugated Polymer Solar Cells Coated*. PhD thesis, Sudan University of Science and Technology, 2015.
- [41] J.C. Hemmelen R. Janssen and N.S. Sariciftci. Polymer-fullerene bulk heterojunction solar cell. *Solid State Physics, 171040 Yulim Jung*, 2006.
- [42] V. Coropceanu, J. Cornil, A. Demetrio F. da Silva, Y. Olivier, R. Silbey, and J.L. Brédas. Charge transport in organic semiconductors. *Chemical reviews*, 107(4):926–952, 2007.
- [43] G. Li, R. Zhu, and Y. Yang. Polymer solar cells. *Nature Photonics*, 6(3):153–161, 2012.
- [44] W. Ge. An overview on p3ht: Pcbm, the most efficient organic solar cell material so far. *Solid State Physics, Spring*, 2009.
- [45] J.L. Brédas, J.E. Norton, J. Cornil, and V. Coropceanu. Molecular understanding of organic solar cells: the challenges. *Accounts of chemical research*, 42(11):1691–1699, 2009.

- [46] W.U. Huynh, J.J. Dittmer, and A.P. Alivisatos. Hybrid nanorod-polymer solar cells. *science*, 295(5564):2425–2427, 2002.